Journal of
Materials Chemistry B

Materials for biology and medicine

Accepted Manuscript

This article can be cited before page numbers have been issued, to do this please use: Z. Zheng, R. Zhu, I. Peng, Z. Xu and Y. Jiang, *J. Mater. Chem. B*, 2024, DOI: 10.1039/D4TB00782D.

This is an Accepted Manuscript, which has been through the Royal Society of Chemistry peer review process and has been accepted for publication.

Accepted Manuscripts are published online shortly after acceptance, before technical editing, formatting and proof reading. Using this free service, authors can make their results available to the community, in citable form, before we publish the edited article. We will replace this Accepted Manuscript with the edited and formatted Advance Article as soon as it is available.

You can find more information about Accepted Manuscripts in the Information for Authors.

Please note that technical editing may introduce minor changes to the text and/or graphics, which may alter content. The journal's standard Terms & Conditions and the Ethical guidelines still apply. In no event shall the Royal Society of Chemistry be held responsible for any errors or omissions in this Accepted Manuscript or any consequences arising from the use of any information it contains.

ROYAL SOCIETY OF CHEMISTRY

rsc.li/materials-b

View Article Online
DOI: 10.1039/D4TB00782D

Wearable and Implantable Biosensors: Mechanisms and Applications for Closed-Loop Therapeutic Systems

Zeyuan Zheng[1], Runjin Zhu[1], Ian Peng[1], Zitong Xu[1] & Yuanwen Jiang[1*]

[1]*Department of Materials Science and Engineering, University of Pennsylvania, Pennsylvania, PA 19104*

**Corresponding author: ywjiang@seas.upenn.edu.*

View Article Online
DOI: 10.1039/D4TB00782D

Abstract

This review article examines the current state of wearable and implantable biosensors, offering an overview of their biosensing mechanisms and applications. We also delve into integrating these biosensors with therapeutic systems, discussing their operational principles and incorporation into closed-loop devices. Biosensing strategies are broadly categorized into chemical sensing for biomarker detection, physical sensing for monitoring physiological conditions such as pressure and temperature, and electrophysiological sensing for capturing bioelectrical activities. The discussion extends to recent developments in drug delivery and electrical stimulation devices to highlight their significant role in closed-loop therapy. By integrating with therapeutic devices, biosensors enable the modulation of treatment regimens based on real-time physiological data. This capability enhances the patient-specificity of medical interventions, an essential aspect of personalized healthcare. Recent innovations in integrating biosensors and therapeutic devices have led to the introduction of closed-loop wearable and implantable systems capable of achieving previously unattainable therapeutic outcomes. These technologies represent a significant leap towards dynamic, adaptive therapies that respond in real-time to patients' physiological states, offering a level of accuracy and effectiveness that is particularly beneficial for managing chronic conditions. The review also addresses the challenges associated with biosensor technologies. We also explore the prospects for these technologies to address their potential to transform disease management with more targeted and personalized treatment solutions.

Keywords: biosensing, real-time monitoring, closed-loop therapy, drug delivery, bioelectrical modulation.

View Article Online
DOI: 10.1039/D4TB00782D

1. Introduction

The advent of wearable and implantable biosensors is revolutionizing medical monitoring and treatment, heralding a new era of closed-loop therapeutic systems. These cutting-edge devices provide continuous, real-time data on various physiological parameters, facilitating a transition from conventional static treatment approaches to more dynamic and adaptive medical interventions. This transformation is driven by the integration of sophisticated sensing mechanisms, their application in therapeutic devices, and the subsequent introduction of innovative closed-loop therapeutic systems. Various sensing mechanisms that monitor physiological states with remarkable sensitivity and specificity are at the heart of these advanced biosensors. These mechanisms can be classified into chemical, physical, and electrophysiological sensing. Chemical sensors, including redox-based, impedance-based, and transistor-based types, excel at detecting biomarkers and metabolic parameters. Physical sensors like pressure and temperature sensors track vital signs and mechanical properties. Electrophysiological sensors capture bioelectrical signals from the brain, heart, and muscles, offering crucial insights into the body's electrical activities. The success of these sensors is anchored in cutting-edge materials and microfabrication technologies that ensure biocompatibility and long-term stability.

The integration of these biosensors into therapeutic devices marks a significant leap forward in personalized medicine. Drug delivery systems, such as microneedles, implantables, and ingestibles, use biosensors to control the release of therapeutic agents based on real-time physiological data. For example, glucose-responsive microneedle patches dynamically adjust insulin release in diabetic patients, mimicking the natural glucose regulation of the pancreas. Similarly, implantable devices for neurological conditions can release medication upon detecting specific bioelectrical signals, providing immediate intervention during events such as seizures. Electrical stimulation devices, enhanced by biosensing capabilities, offer targeted therapeutic effects by applying controlled electrical currents to tissues. Innovations such as self-powered electronic bandages accelerate wound healing while integrating sophisticated sensing mechanisms drives bioelectronics, and their application interfaces enable precise neuromodulation with minimal

View Article Online
DOI: 10.1039/D4TB00782D

invasiveness. These applications demonstrate biosensors' capacity to monitor and actively modulate physiological states to enhance the efficacy of medical interventions. Looking ahead, the potential of biosensors to transform disease management with more targeted and personalized treatment solutions is immense, promising a future of improved healthcare.

Integrating biosensors with drug delivery and electrical stimulation devices introduces closed-loop therapeutic systems. These systems interconnect biosensors and therapeutic devices to autonomously adjust treatment regimens based on instantaneous physiological feedback, thus ensuring optimal therapeutic outcomes. This approach is particularly advantageous for managing chronic conditions, where maintaining drug concentrations within a specific therapeutic window is crucial for long-term treatment. For example, theranostic contact lenses monitor intraocular pressure and deliver anti-glaucoma medication on demand. Similarly, prosthetic systems with electronic dermis provide sensory feedback, mimicking natural skin responses and enhancing user experience. By embedding biosensors into these advanced systems, closed-loop devices can achieve therapeutic outcomes previously unattainable with static treatments. They offer dynamic, patient-centered solutions that continuously adapt to the individual's physiological state, revolutionizing disease management and treatment personalization.

The integration of sensing mechanisms into wearable and implantable biosensors, drug delivery systems, and electrical stimulation devices is driving the evolution of closed-loop therapeutic systems. This review covers these systems' operational principles, recent advancements, and the challenges and opportunities presented by these technologies.

View Article Online
DOI: 10.1039/D4TB00782D

2. Sensing Strategies

Biosensing strategies can be divided into three main categories: chemical sensing for detecting biomarkers, physical sensing for tracking physiological conditions like pressure and temperature, and electrophysiological sensing for recording bioelectrical activities. (Table 1).

2.1 Chemical Sensing

Chemical sensing detects chemical substances by leveraging the specificity of biological interactions. This domain encompasses redox-based, impedance-based, and transistor-based chemical sensors, each utilizing distinct mechanisms to transduce biological recognition events into measurable signals[1-3]. These methodologies enable the direct and indirect detection of a wide range of analytes.

The primary importance of chemical sensing lies in its ability to track biomolecules. Recent developments in chemical biosensors allow for continuous detection of a range of biomarkers to enable quantification of different metabolites, medications, hormones, electrolytes, and proteins in blood and biofluids[3-5]. Biomarkers are important biophysical indicators of physiological states, disease processes, or pharmacodynamical responses. They facilitate the diagnosis and prognosis of diseases and monitor the effectiveness of therapeutic interventions. The integration of chemical sensing and biomarker analysis offers a direct view of the body's biochemical dynamics and marks a significant advancement in personalized medicine.

2.1.1 Redox-based Biorecognition

Reduction-oxidation reaction is a chemical process involving electron transfer between two species. It is the primarily utilized mechanism of amperometric and voltammetric sensors[4, 6-8]. These sensors use an applied voltage potential to facilitate electron transfer between the biomarker and electrode, generating an electrical current proportional to the analyte concentration in the sample. The core of an amperometric biosensor is its electrode system, typically consisting of a working electrode, a reference electrode, and a counter electrode. The working electrode is where the redox reaction of interest occurs, the

View Article Online
DOI: 10.1039/D4TB00782D

reference electrode maintains a constant potential, and the counter electrode completes the circuit. To achieve selectivity for the target analyte, the working electrode is often modified with specific biological recognition elements, such as enzymes, antibodies, aptamers, or deoxyribonucleic acid (DNA), which bind selectively to the target molecule[9-11].

Enzymatic redox sensors exploit the catalytic specificity of enzymes to facilitate the quantitative analysis of targeted analytes within complex biological matrices[8, 12, 13]. The operational principle of these devices hinges on the immobilization of a specific enzyme onto the conductive surface of an electrode. This procedure necessitates retaining the native conformational and catalytic properties of the enzyme while ensuring its stable integration within the electrochemical environment. Upon exposure to the target analyte, the immobilized enzyme catalyzes a substrate-specific reaction to form electroactive species or consume electroactive reactants. This biochemical transformation initiates a redox reaction at the electrode interface, culminating in the transduction of a chemical signal into a quantifiable electrical current. The magnitude of this current is directly proportional to the analyte's concentration within the sample, which provides a basis for quantitative analysis[3]. Advancements in enzymatic sensor design have led to the development of third-generation sensors[14, 15]. These sensors use direct electron transfer mechanisms between the enzyme active site and the electrode to circumvent the need for exogenous mediators, thereby enhancing the sensor's analytical specificity and reducing its susceptibility to interfering substances.

In glycemic control, the enzyme glucose oxidase (GOx) catalyzes the specific oxidation of glucose to gluconic acid, concomitantly generating hydrogen peroxide. Subsequent electrochemical oxidation of this byproduct generates a quantifiable current reflecting glucose concentration[16-18]. This mechanism underscores the clinical relevance of GOx-based sensors in the real-time monitoring of glucose levels, an essential parameter in diabetes management[19, 20]. Conversely, lactate oxidase (LOx) exemplifies another enzyme utilized in amperometric sensors[21, 22]. It catalyzes the conversion of lactate to pyruvate and hydrogen peroxide. Subsequently, the oxidation of hydrogen peroxide at the electrode surface generates a current proportional to lactate concentration, providing data for clinical diagnostics, metabolic rate analysis, and patient monitoring in critical care settings. Gao et al. introduced a wearable sensor array enabling

View Article Online
DOI: 10.1039/D4TB00782D

simultaneous quantification of sweat metabolites (glucose, lactate), electrolytes (Na^+, K^+), and temperature[23]. This system integrates plastic-based sensors with silicon circuits on a flexible substrate, resolving limitations associated with single analyte detection and the absence of on-site signal processing. Amperometric sensors utilizing glucose oxidase and lactate oxidase within a chitosan matrix and a shared Ag/AgCl electrode facilitate metabolite quantification.

The PETAL sensor patch, designed by Zheng et al., utilizes five different colorimetric sensors to monitor critical biomarkers associated with wound healing[24]. Each sensor operates on a distinct sensing mechanism tailored to detect specific wound-related parameters: temperature, pH, trimethylamine (TMA), uric acid (UA), and moisture (Fig. 1A). The temperature sensor, made of cholesteric liquid crystals, changes color from red to green to blue as temperature increases from 31°C to 36°C, crucial for detecting infection-related temperature rises. The pH sensor, using phenol red dye, shifts from yellow to magenta based on pH levels, indicating wound biochemical environment changes (Fig. 1B). The TMA sensor employs Reichardt's solvatochromic dye, which changes from dark gray to light white in the presence of TMA, a bacterial infection marker. The UA sensor uses an enzymatic reaction involving uricase and peroxidase, producing a dark pink color correlated with UA levels, indicating prolonged inflammation or infection (Fig. 1B). The moisture sensor relies on anhydrous cobalt chloride in a polyvinyl alcohol matrix, changing from deep blue to pink as moisture levels increase, ensuring sufficient exudate reaches the sensor. These sensors are integrated into a wax-printed paper fluidic panel arranged in a five-petaled flower pattern, allowing equal channeling of wound exudate to each detection zone. AI-enabled data analysis, performed through deep learning algorithms on smartphone-captured images, classifies wound status and provides early warnings for adverse events, triggering treatments like antibiotics for infections or anti-inflammatory measures. The control module, comprising the smartphone and neural network, enables real-time monitoring and treatment, forming a closed-loop system where wound exudate is channeled to the sensor, data is analyzed, and appropriate treatments are administered. This system's logical flow diagram involves continuous monitoring, data capture, analysis, and treatment, ensuring effective wound management. The

View Article Online
DOI: 10.1039/D4TB00782D

PETAL sensor patch offers holistic, non-invasive, and rapid wound monitoring, leveraging diverse sensing mechanisms and AI-driven analysis to enhance clinical wound care and management.

Aptamers, synthesized as single-stranded oligonucleotides or peptides, have emerged as pivotal biological recognition elements in the development of redox sensors[10, 25]. Derived through the systematic evolution of ligands by exponential enrichment, these entities exhibit a high degree of specificity and affinity for their respective targets[26, 27]. This specificity is attributable to their ability to fold into unique tertiary structures, enabling selective binding to a diverse range of analytes, from small ions to large macromolecules (Fig. 1C)[28].

In electrochemical biosensing, aptamers are the functional biorecognition interface within redox sensors. The fundamental mechanism of these aptamer-based sensors, or aptasensors, involves immobilizing an aptamer onto an electrode surface[29-31]. The binding of the target analyte induces a conformational change in the aptamer, which in turn influences the electron transfer process between the electrode and a coupled redox-active reporter (Fig. 1D)[28]. This interaction can be quantitatively monitored through alterations in the electrochemical signal, directly correlating with the concentration of the target analyte (Fig. 1C). Two predominant strategies define the operational principles of aptasensors: binding-induced conformational alteration and target-induced displacement[32-34]. In the former, the structural rearrangement of the aptamer upon target binding modulates the proximity of a redox-active reporter to the electrode, thereby affecting the electron transfer rate. In the latter, the binding event leads to the displacement of a complementary strand, tagged with a redox-active reporter, altering the electrochemical signal. Illustrative of the application of aptamers in redox sensors is the thrombin aptasensor[35]. Here, a thrombin-specific aptamer is anchored onto a gold nanoparticle-modified electrode. Upon thrombin binding, the aptamer transitions into a G-quadruplex structure, modifying the spatial relation to a methylene blue reporter and thus enhancing the electrochemical signal in proportion to the thrombin concentration.

Antibodies, or immunoglobulins, have long been integral to the biochemical toolkit due to their unparalleled specificity and affinity for antigenic targets[36-39]. This specificity is derived from the antibodies' unique structure, allowing them to recognize epitopes with high precision. Integrating antibodies into redox

View Article Online
DOI: 10.1039/D4TB00782D

sensors leverages their immunological binding capabilities to detect a wide range of substances, from small molecules to proteins and cells, with significant implications for diagnostics and analytical chemistry. The operational mechanism of antibody-based redox sensors typically involves the immobilization of antibodies on the surface of an electrode[37, 38, 40]. This immobilization must preserve the antibody's antigen-binding affinity and orientation while facilitating electron transfer for signal transduction. Upon antigen binding, the antibody-antigen interaction can either directly affect the electron transfer process at the electrode interface or be coupled with a secondary reaction that produces an electroactive species, measurable via standard electrochemical techniques.

One exemplary antibody application in redox sensors is the detection of the cardiac biomarker troponin[41-44]. Gholami introduces a new electrochemical immunosensor for detecting human cardiac troponin I (cTnI) in blood plasma, leveraging a conductive polymer deposited on an indium tin oxide electrode[45]. Anti-cTnI antibodies are immobilized on the polymer for specific cTnI binding, while $[Fe(CN)_6]^{3-/4-}$ was used as a redox probe to transfer single electrons onto the sensing interface. Detection relies on differential pulse voltammetry to measure current changes when cTnI binds. Another application involves the use of antibodies in the construction of sensors for the detection of the hormone insulin[46]. Antibodies against insulin are anchored onto the electrode surface. Upon interaction with insulin molecules, a change in the electrochemical environment near the electrode surface occurs, which can be detected as a change in current. This configuration can be further refined by employing a label-free format, where insulin binding to its antibody directly influences the electron transfer properties at the electrode interface, providing a quantitative measure of insulin levels. Such sensors are invaluable for monitoring glucose and insulin levels in diabetic patients, contributing to better disease management and therapeutic strategies[47].

Thompson et al. designed a novel biosensor system that utilizes antibody switches for continuous, in situ quantification of small-molecule analytes[48]. This mechanism leverages a DNA scaffold to tether antibodies to a molecular antagonist, thereby inducing antigen-specific conformational alterations that manifest as quantifiable fluorescence shifts through Förster resonance energy transfer (FRET) (Fig. 1E). The proof-of-concept is substantiated with digoxigenin and cortisol, demonstrating the platform's capacity

View Article Online
DOI: 10.1039/D4TB00782D

for on-demand detection in undiluted plasma. Sensitivity is achieved by altering the molecular antagonist, thus extending detection thresholds from the nanomolar to the millimolar spectrum. Further, coupling with a fiber optic sensor apparatus facilitates uninterrupted, real-time cortisol monitoring in buffer and blood matrices. For digoxigenin, a dynamic response range of ~100 nM to 1 mM is recorded, while for cortisol, sensitivity enhancement is achieved through strategic antagonist substitution, enabling detection over physiologically relevant concentrations.

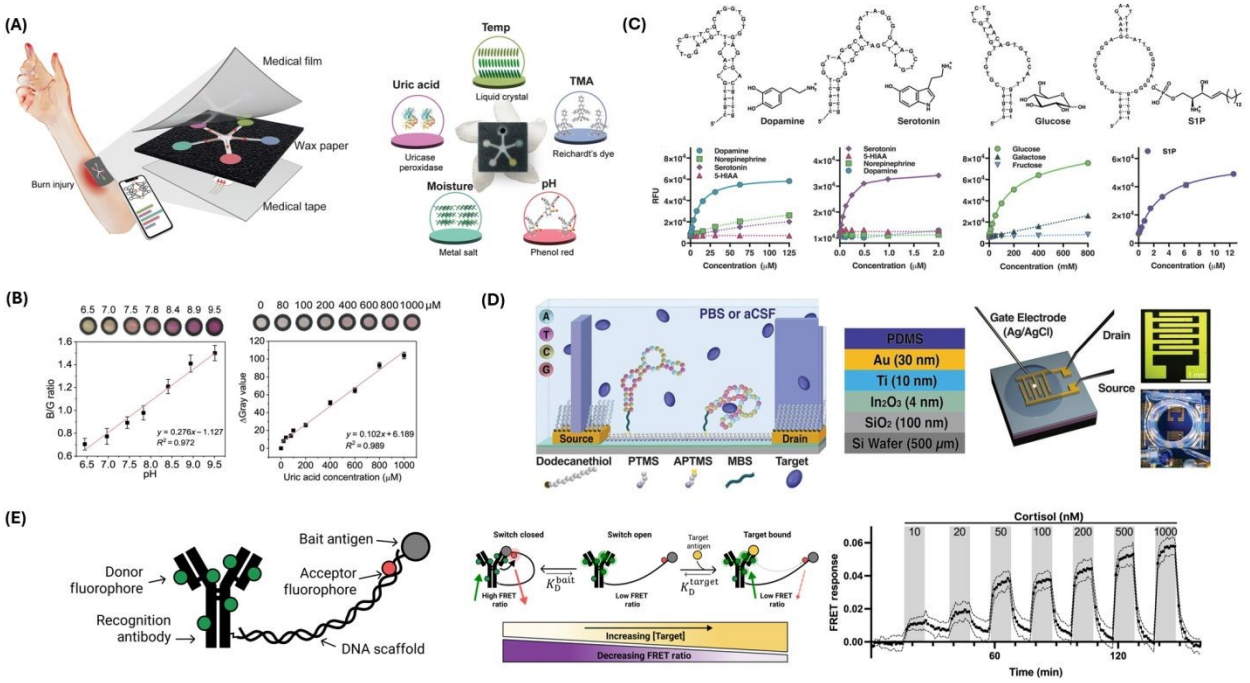

Figure 1. Chemical sensing strategies for biomarker detection. (A) Illustration of PETAL sensor comprising temperature, pH, trimethylamine, uric acid, and moisture sensors for colorimetric analysis of wound healing status. Sensor patch displays the sensing materials/principles of each sensor. Reproduced from reference 24 with permission from *The American Association for the Advancement of Science (AAAS)*, copyright 2023. **(B)** Representative calibrations showing the pH and uric acid sensors. Reproduced from reference 24 with permission from *AAAS*, copyright 2023. **(C)** Aptamers for dopamine, serotonin, glucose, and sphingosine-1-phosphate, and their respective responses detected by aptasensors. Reproduced from reference 28 with permission from *AAAS*, copyright 2018. **(D)** Schematic of FET sensor surface chemistry (left). PTMS: trimethoxy(propyl)silane; APTMS: (3-aminopropyl) trimethoxysilane; MBS: 3-maleimidobenzoic acid N-hydroxysuccinimide ester. FET experimental setup (right). Reproduced from reference 28 with permission from *AAAS*, copyright 2018. **(E)** Antibody-switch design and mechanism. Antibody is engineered into a molecular switch by tethering it to a bait molecule using DNA scaffold (left). The molecular switch functions via a competitive balance (middle). Higher concentrations of the target move the equilibrium in favor of the target-bound state and away from the closed state. Upon binding with the target, the switch shows a reduced FRET ratio. Continuous monitoring of cortisol levels is shown from10 nM to 1 μM, measured by functionalized fiber optic sensors (right). Reproduced from reference 48 with permission from *AAAS*, copyright 2023.

2.1.2 Impedance-based Chemical Sensors

View Article Online
DOI: 10.1039/D4TB00782D

Impedance-based biosensors leverage the principles of electrochemical impedance spectroscopy (EIS)[49-51]. These devices operate by measuring the impedance change in an electrochemical cell attributed to the biochemical interactions occurring at the sensor interface.

Impedance-based biosensors can be classified into faradaic and non-faradaic types[52]. Faradaic impedance-based biosensors rely on electron transfer reactions between the analyte and the electrode surface[53]. This transfer affects the system's impedance in a manner directly correlated to the analyte concentration. In these sensors, the faradaic processes are marked by redox activities, where the electrochemical reactions at the electrode-electrolyte interface are integral for sensor functionality. These interactions, typically represented through Nyquist plots, delineate the charge transfer resistance and double-layer capacitance, offering insights into the electrochemical kinetics and the interface's physical properties. In contrast, non-faradaic impedance biosensors detect changes in impedance without involving redox reactions[52]. These sensors exploit variations in the dielectric properties and conductivity at the sensor interface induced by the binding of target molecules. The absence of faradaic processes eliminates the need for redox-active species, thus broadening the application of these sensors in bio-sensing, especially where redox-active elements can interfere with the analyte detection or are inherently absent. This property makes non-faradaic impedance biosensors potentially advantageous for developing closed-loop systems. This label-free detection simplifies sensor design and reduces the risk of interference from other substances[54]. For example, the commonly used redox probe (Ferro/Ferricyanide $[Fe(CN)6]^{3-/4-}$) can denature protein biomarkers due to its toxicity [55].

The design and fabrication of impedance-based biosensors incorporate several critical components: electrodes, electrolytes, and recognition elements[50, 51]. The electrodes, typically constructed from conductive materials like gold, carbon, or platinum, are designed to facilitate effective electron transfer and to withstand the physicochemical conditions of the sensing environment. The interfacial properties of these electrodes, essential for sensitivity and selectivity, are often modified with biological recognition elements such as antibodies, DNA strands, or enzymes[50, 56]. These biomolecules are immobilized on the electrode's surface, enabling the selective capture of target analytes from complex biological matrices.

View Article Online
DOI: 10.1039/D4TB00782D

One example of a non-faradaic impedance-based sensor is used for the label-free detection of glucose in sweat[57]. In this sensor, EIS measures impedance changes resulting from glucose's interaction with immobilized glucose oxidase antibodies on the sensor's surface. This interaction modulates the properties of the electrical double layer at the ZnO electrode-electrolyte interface, affecting its capacitance and resistance without relying on the direct electrochemical oxidation or reduction of the glucose. This approach affords several advantages, including the absence of a need for redox-active intermediates or labels, and a reduction in the potential for interference from other substances present in sweat that might undergo faradaic reactions. Another example of an impedance-based non-faradaic sensor is the development of an immunosensor for the ultrasensitive detection of interleukin-6 (IL-6)[58]. This sensor integrates gold nanoparticles (AuNPs) electrochemically deposited on an array of single-walled carbon nanotubes (SWCNTs), combining the enhanced conductivity and surface area of SWCNTs with the efficient electron transfer properties of AuNPs to facilitate the immobilization of IL-6 antibodies. The detection mechanism operates on the principle that the specific binding of IL-6 antigens to antibodies alters the charge transfer resistance (Rct) at the electrode-electrolyte interface, measurable via EIS.

2.1.3 Transistor-based Chemical Sensors

In transistor-based biosensors, the field-effect transistor (FET) is the critical component for converting biomolecular interactions into quantifiable electrical signals[2, 59, 60]. The key mechanism involves modulating the FET's channel conductivity in response to the binding of target biomolecules to the gate area, altering the electric field and thereby affecting the flow of charge carriers between the source and drain terminals. This interaction induces a measurable change in the drain-source current, directly correlating with the concentration of the analyte. Design advancements focus on enhancing the transistor's sensitivity and specificity. Utilization of materials with high electron mobility, such as graphene, for the channel and precision in the immobilization of bio-recognition elements on the gate surface are central strategies[60, 61]. These elements, whether enzymes or antibodies are anchored onto the gate area to specifically capture target molecules, significantly influencing the transistor's electrical response to the biological event[2, 59, 62].

View Article Online
DOI: 10.1039/D4TB00782D

There are various types of transistor-based biosensors[60]. Ion-sensitive field-effect transistors (ISFETs) operate by detecting changes in ion concentration adjacent to their gate surfaces, which directly influences the device's threshold voltage[60, 63]. This capability is exploited for pH measurement and extended toward specific ion detection through surface functionalization. The ion concentration modulates the surface potential at the semiconductor-liquid interface, affecting the channel conductivity and, thus, the ISFET's output signal. Silicon nanowire biosensors utilize the high surface-to-volume ratio and semiconducting properties of silicon nanowires to detect biomolecular binding events[60, 64]. These biosensors are sensitive to surface charge alterations induced by the adsorption of biomolecules, leading to modulation in nanowire conductance. This sensitivity allows for the detection of nucleic acids, proteins, and other biomolecules at low concentrations, leveraging the intrinsic electronic properties of silicon nanowires for biosensing applications. The operational mechanism of organic FET (OFET) biosensors is predicated on the modulation of conductivity in an organic semiconductor channel by biomolecular interactions at the gate electrode[60, 65]. Target biomolecule binding to a biorecognition layer alters the surface potential, impacting the charge carrier mobility within the organic semiconductor. This results in a quantifiable change in the OFET's electrical output, allowing for the detection of specific biological analytes. The inherent flexibility of organic semiconductors facilitates the development of wearable and implantable biosensors. Graphene FET (GFET) biosensors utilize the electrical conductivity and surface area of graphene[60, 66]. Biomolecule adsorption onto the graphene surface leads to changes in its electrical properties, such as carrier concentration or mobility, due to the biomolecular binding. These changes can be directly correlated with the presence and concentration of the target analyte. GFETs are particularly noted for their ultra-high sensitivity and specificity in biomolecule detection, making them ideal candidates for developing advanced biosensing platforms.

Many studies have reported on the use of transistor-based biosensors to measure protein and DNA levels and research cell physiology. One report discusses the development and optimization of organic thin-film transistor (OTFT) biosensors, focusing on their sensitivity to pH variations and DNA concentrations for effective DNA detection[67]. The core of the sensing mechanism involves the hybridization of DNA to

View Article Online
DOI: 10.1039/D4TB00782D

peptide nucleic acid sequences immobilized on the OTFT surface. This interaction modulates the OTFT's electrical characteristics, specifically the drain-source current, by influencing the electric field at the semiconductor-liquid interface due to the charge of the hybridized DNA. The OTFT biosensors employ the organic semiconductor DDFTTF for its stable mobility in buffer solutions. A key aspect of the study is the impact of gate-bias stress, attributed to the migration of counter-ions from the electrolyte into the organic film, on the stability and sensitivity of the biosensor. Adjustments in pH toward physiological conditions are shown to mitigate this stress, enhancing the sensor's ability to detect DNA.

Furthermore, a glucose biosensor based on organic electrochemical transistors (OECTs) was developed utilizing platinum gate electrodes modified with enzyme and nanomaterials[68]. The core sensing mechanism of these biosensors involves GOx-modified Pt gate electrodes, enhanced significantly by incorporating nanomaterials such as multi-wall carbon nanotubes or platinum nanoparticles (Pt-NPs). The transistor's operation leverages the catalytic reaction facilitated by GOx, which oxidizes glucose to produce gluconolactone and hydrogen peroxide (H_2O_2). The generation of H_2O_2 alters the local electrochemical environment at the gate electrode, which, in turn, modulates the conductivity of the OECT channel. This change in conductivity is measurable as a variation in the current between the source and drain electrodes of the transistor, correlating directly with glucose concentration.

Nakatsuka et al. introduced a novel approach to overcoming the Debye length limitation in FET-based biosensors, a critical barrier in the detection of small molecules under high–ionic strength conditions typical of physiological environments[69]. By incorporating aptamers with specific stem-loop structures that undergo conformational changes upon target binding, the study demonstrates enhanced sensitivity in the detection of various small molecules including charged and electroneutral targets such as serotonin, dopamine, glucose, and sphingosine-1-phosphate (Fig. 1C). The sensing mechanism of these aptamer-modified FETs relies on target-induced conformational changes of the aptamer's negatively charged phosphodiester backbone, situated in proximity to the semiconductor channels (Fig. 1D). These conformational changes gate the conductance in physiological buffers, enabling the detection of targets at ultra-low concentrations. Notably, this method sidesteps the traditional Debye screening effect by

View Article Online
DOI: 10.1039/D4TB00782D

leveraging the spatial rearrangement of charged aptamer segments upon target binding, thus effectively amplifying the signal for FET sensors. Fabrication of the devices involved printing ultrathin metal-oxide FET arrays and modifying them with deoxyribonucleotide aptamers selected for adaptive binding to their respective targets.

2.1.4 pH-Responsive Chemical Sensors

pH-responsive chemical sensors are an essential class of biosensing devices designed to detect and monitor changes in the pH levels of their environment. These sensors exploit the unique properties of pH-sensitive materials, which undergo measurable physical or chemical transformations in response to variations in hydrogen ion concentration. Common sensing mechanisms include the swelling or contraction of hydrogels, changes in optical properties such as color or fluorescence, and alterations in electrical properties like impedance or conductivity[70]. These transformations are transduced into quantifiable signals, allowing for accurate monitoring of pH. Such capability is essential in numerous biomedical applications, including the detection of metabolic imbalances, monitoring of wound healing, and early diagnosis of pathological conditions such as cancer and infections[71]. Recent advancements in material science have led to the development of susceptible and biocompatible pH-responsive sensors that can be integrated into wearable and implantable devices, enabling continuous and non-invasive monitoring of physiological pH levels. These innovations hold significant promise for enhancing personalized healthcare and improving patient outcomes by providing real-time data for timely medical interventions.

Innovations in bioresorbable materials have led to developing shape-adaptive structures capable of real-time, non-invasive monitoring of deep-tissue pH homeostasis using conventional ultrasound imaging. Liu et al. present a mechanism for this advanced monitoring system[72]. The system, termed BioSUM, integrates small bioresorbable metal disks within pH-responsive hydrogels, which swell or contract in response to local pH changes. This swelling alters the spacing between the metal disks, which is detectable via ultrasound imaging. This method allows for precise monitoring of characteristics such as pH-induced dimensional changes. The required functions measured by these sensors include local pH and associated physiological perturbations. In cases where the monitoring detects abnormalities, such as leaks in

View Article Online
DOI: 10.1039/D4TB00782D

gastrointestinal surgeries, immediate therapeutic interventions are necessary. Treatments may involve surgical corrections or administration of medications to manage complications. The system's control module integrates real-time data acquisition, analysis, and intervention, enabling seamless monitoring and treatment. The logical flow diagram of this system involves continuous pH measurement, data transmission to the control unit, analysis for deviations from homeostasis, and activation of therapeutic protocols as needed, ultimately enhancing patient care by providing timely and accurate assessments while eliminating the need for secondary surgical procedures due to the bioresorbable nature of the materials used.

Another study shows a development in bioresorbable nanostructured chemical sensors for in vivo pH monitoring. This design by Corsi et al. leverages a sophisticated sensing mechanism based on the dynamic swelling and shrinking of a polymer multilayer stack conformally coated on a porous silica membrane[73]. This sensor meticulously monitors pH characteristics by employing alternating layers of polyelectrolytes labeled with a pH-insensitive fluorophore, Rhodamine-B, whose fluorescence intensity changes linearly with pH due to the swelling and shrinking of the polymer layers, thereby affecting fluorescence quenching. This detailed and responsive mechanism enables real-time, continuous measurement of pH changes within the physiological range of 4 to 7.5, crucial for monitoring conditions such as inflammation, cancer progression, or tissue acidosis. Upon detecting significant pH alterations, the sensor data can prompt necessary treatments, such as localized drug delivery or pH modulation therapies, through a control module that manages these responses. The control module functions as the central component of a closed-loop system, continuously analyzing sensor data and initiating appropriate therapeutic interventions. The application flow of this system includes the sensor detecting pH changes, the control module processing this data, and subsequently activating the necessary treatments, ensuring a responsive and adaptive approach to patient care.

2.2 Physical Sensing

2.2.1 Pressure Sensing

The pressure inside the human body, such as intraocular pressure, intracranial pressure, and blood pressure, is critical in diagnosing physiological health and anticipating injuries[74]. In recent years, pressure

View Article Online
DOI: 10.1039/D4TB00782D

sensors applicable to closed-loop therapeutic devices utilizing various physical effects have been developed. Capacitive approaches are well-developed for biomedical pressure sensing, which could be used for closed-loop therapeutic devices. Capacitive pressure sensors can be designed in a thin and flat form factor, capable of sensing pressure normal to the sensor plane with low invasiveness. One typical approach of capacitive pressure sensors for biomedical devices utilizes microstructured compressible electrodes. Stacked under a dielectric layer and a flat electrode, the contact area between the bottom microstructured compressible electrode and the dielectric layer increases as the normal pressure applied to the sensor increases; thus, the capacitance between the flat and microstructured electrodes[75].

Several pressure sensors have been designed using this approach. For example, a flexible capacitive sensor was created by Yang et al[76]. Fabricated with a CO_2 laser with a Gaussian beam profile, the sensor had an optimized gradient pyramidal microstructure with an individually controlled profile and height of each pyramid. The micropyramid profile and non-uniform micropyramid height gradient enabled excellent linearity over a broad pressure range, and high sensitivity was achieved with a thin ionic liquid layer as the dielectric layer. Lin et al. developed a thin and flexible capacitive pressure sensor consisting of a layer of ionic liquid-coated fabric as the dielectric layer sandwiched between two flat electrodes[77]. As the normal pressure applied to the sensor increased, the contact area between the fabric and the electrodes increased, boosting the capacitance between the electrodes by up to a few orders. This design enables the sensor to utilize fingertips as a platform for pulse monitoring for cardiovascular health evaluation, especially where the pressure was often too weak to be detected by flexible sensors. The sensor monitors key pulse characteristics, including amplitude, rate, and waveform, which are essential for assessing cardiovascular health. The system can be programmed to administer specific treatments or alert medical professionals based on these readings. A control module oversees continuous monitoring and data analysis, ensuring appropriate actions are taken in response to sensor data. The logical flow of the system includes data acquisition, signal processing, anomaly detection, decision-making, and therapeutic intervention execution.

View Article Online
DOI: 10.1039/D4TB00782D

When integrated into a closed-loop system, this sensor could facilitate real-time monitoring, enabling timely interventions when abnormal pulse patterns indicative of cardiovascular issues are detected.

A nanomesh capacitive pressure sensor was engineered by Lee et al. that features an ultrathin design with four layers: a polyurethane nanomesh-embedded passivation layer, top and bottom gold nanomesh electrode layers, and a perylene-coated polyurethane nanomesh intermediate layer (Fig. 2A)[78]. This structure demonstrates mechanical durability and sensitivity, capable of enduring extensive shearing and friction while measuring pressure through capacitance changes caused by the deformation of the intermediate layer. The sensor's sensitivity can be adjusted by varying the number of supporting polyvinyl alcohol nanofibers. The sensor demonstrated optimized durability, with less than 0.15% performance degradation after 1000 pressing cycles at 19.6 kPa and less than 9.7% sensitivity change under high friction. In an object-grasping experiment, the sensor-equipped fingers showed no significant difference in grip force compared to bare fingers, validating the sensor's minimal impact on touch sensation. Lee et al. also showed increased grip force because of varying object shape and mass, as measured by the nanomesh sensor. This design is significant for applications requiring precise, non-intrusive monitoring of finger movements, such as in prosthetics, human-machine interfaces, and hand function restoration.

Su et al. presented another strategy for designing stretchable and strain-unperturbed capacitive pressure sensors (Fig. 2B)[79]. Pressure sensing was achieved by an ionic elastomer layer with specifically stiffened micropyramids. By this design, most of the strain was absorbed by the connective ionic elastomer layer, leaving the shape of the micro pyramids mostly unaffected by strain. Consequently, the sensor exhibited 98% strain insensitivity for strains up to 50% while maintaining a low detection limit of 0.2 Pa. Demonstrating remarkable durability and robustness, those strain-unperturbed capacitive pressure sensors could be utilized by closed-loop therapeutic devices, offering precise monitoring capabilities without the interference typically caused by strain.

In addition to capacitive approaches, the piezoelectric effect is commonly utilized for pressure sensing. Piezoelectric pressure sensors directly transform deformation into electrical charge, eliminating

View Article Online
DOI: 10.1039/D4TB00782D

the need for a power supply to the sensor[74]. Yin et al. developed a piezoelectric self-powered, rapid-response flexible pressure sensor for wearable applications[80]. The sensor employed a 3x3 array of ZnO piezoelectric transducers connected in series and parallel to enhance its output voltage compared to traditional thin-film piezoelectric sensors while maintaining the same film thickness. The sensor demonstrated high linear sensitivity, high durability, and low response and recovery times that further decreased as the dynamic pressure increased. The sensor's practical applications were demonstrated by elbow flexure and finger tapping, which indicates its potential for integration into wearable devices. Min et al. developed a wearable piezoelectric pressure sensor for continuous non-invasive blood pressure monitoring[81]. Attached to a patient's wrist via a medical-grade adhesive layer, the sensor measured tiny pulse waves from the radial artery. Using a linear regression model, the sensor input was converted to blood pressure values. The sensor's accuracy in blood pressure monitoring was demonstrated, with mean differences of -0.89 ± 6.19 and -0.32 ± 5.28 mmHg for systolic and diastolic blood pressure compared to that of a US Food and Drug Administration (FDA)-approved sphygmomanometer, respectively.

Despite the extensive development, capacitive and piezoelectric pressure sensors typically only sense pressure in the normal direction across the broad sensing areas without precision control[82]. On the other hand, 3-axis pressure sensing can be achieved with optical approaches, translating sensor deformation to changes in the light signal[82, 83]. Combined with image sensors, high spatial resolution can also be achieved by optical pressure sensors[82, 83]. Wang et al. developed an optical pressure sensor in thin film form, capable of three-axis pressure sensing at multiple points in the sensing area (Fig. 2C)[82]. The sensor consisted of a flexible imager, a translucent porous rubber layer, and a flexible backlight layer. The flexible backlight layer illuminated multiple light spots onto the imager, whose intensity distribution changed when subject to normal pressure and shifted away from their neutral position when subject to tangential pressure. By curve fitting the imager readout to the 2D Gaussian function, the amplitude and direction of pressure applied to the light spot could be detected.

2.2.2 Temperature Sensing

View Article Online
DOI: 10.1039/D4TB00782D

Temperature is a vital sign of human health and a key marker for many pathological conditions. Thermal resistive, thermal electric, and temperature sensors utilizing other physical effects have been developed to be suitable for closed-loop therapeutic devices.

Thermal resistive sensors are commonly used for biomedical applications for their high precision and sensitivity. The resistance of the sensing component is temperature-dependent and can be electrically read out. Lu et al. developed a fiber-shaped flexible thermal resistive temperature sensor with NiO nanosheet-coated carbon nanotube fiber (CNTF) composite material as the temperature sensing component (Fig. 2D)[84]. The fabrication of the composite material was made possible with a novel two-step synthetic method, loading Ni hydroxide on the surface of CNTF, followed by in situ decomposition of Ni hydroxide into NiO by chemical vapor decomposition. The sensor combined the high-temperature sensitivity of NiO and the excellent flexibility of CNTF. The authors demonstrated wearable applications of the sensor by monitoring the contact temperature of the human skin, as well as respiration signal monitoring by attaching the sensor to a mask.

For example, Dan and Elias developed a flexible and stretchable resistive temperature sensor. A composite of poly(hydroxybutyrate) with reduced graphene oxide as the nanofiller was synthesized as the sensing component[85]. The sensor showed high sensitivity and resistance to pressure and moisture. The composite was compatible with multiple fabrication techniques, including drop-coating and direct ink writing, and could be patterned on flexible and stretchable substrates, like polyethylene terephthalate. The authors demonstrated the versatility of the temperature sensor by fabricating an array of temperature sensors for thermal mapping. Fan et al. developed a thermal resistive temperature sensor for wearable applications that are invulnerable to sweat interference. Poly(3,4-ethylenedioxythiophene)–poly(styrenesulfonate) (PEDOT:PSS) fiber was chosen as the sensing component for its temperature-sensitive electrical conductivity[86]. Sweat resistance was provided by polyurethane/graphene composite encapsulation while maintaining sensitivity. The sensor is capable of real-time monitoring of body temperature to offer high sensitivity and rapid response time. The sensor could be woven into fabrics and integrated with textile

View Article Online
DOI: 10.1039/D4TB00782D

electronics, making it suitable for wearable applications, and could be utilized by closed-loop therapeutic devices.

Despite the extensive development, the sensing mechanism of thermal resistive temperature sensors necessitates active powering, making long-term temperature monitoring challenging [87]. Additionally, the operation of thermal resistive temperature sensors generates heat at measurement sites, degrading the reliability of the temperature measurement. To address such a challenge, the thermoelectric effect (TE) can be utilized, directly converting temperature difference to voltage [88]. While traditional thermocouples are often unsuitable for closed-loop therapeutic devices for their bulky form factors and invasiveness, novel TE temperature sensors have been developed to address such challenges [89].

Yu et al. developed a TE temperature sensor incorporating 3D spiral thermoelectric Bi_2Te_3 films [87]. The 3D spiral structure of the Bi_2Te_3 films optimized the length of the heat diffusion route and thermal impedance, enabling rapid response while still being able to maintain sufficient temperature difference across the sensor. Combined with the high Seeback coefficient of Bi_2Te_3, the sensor demonstrated high-temperature sensitivity. The performance of the TE temperature sensor made it a promising candidate for future studies on closed-loop therapeutic devices. Wang et al. developed a flexible TE temperature sensor using graphene fibers synthesized through a microfluidic spinning technique and vitamin C reduction[90]. The sensor demonstrated high sensitivity, high electrical conductivity, flexibility, and good scalability in length. Due to its robust performance under bending and length variation, it has the potential for real-time human body temperature monitoring.

In recent years, frequency output temperature sensors gathered increasing interest. With a temperature-dependent oscillation frequency as output, those temperature sensors enable simple integration with digital systems and wireless transmission and are insensitive to electromagnetic interference [91]. Zamora-Mejia at al. designed a passive frequency output temperature sensor for biomedical temperature monitoring[92]. Utilizing a high frequency 860-960 MHz radio frequency radio frequency (RF) carrier for data transmission and energy harvesting, the sensor was wireless and battery-free, showing a wide read

View Article Online
DOI: 10.1039/D4TB00782D

range with low power consumption, suitable for wearable and implantable closed-loop therapeutic devices. Shi et al. engineered an implantable miniaturized frequency output temperature sensor with a volume of only 0.065 mm3, capable of wireless ultrasonic energy harvesting and telemetry[89]. The extremely low volume reduced the device's invasiveness, enabled access to limited interstitial spaces, and simplified the implantation process to solely injection. The device consisted of a monolithically integrated relaxation oscillator temperature sensor and a lead zirconate titanate piezoelectric transducer. When ultrasound was applied to the implanted device via an external ultrasound imager, the piezoelectric transducer harvested energy from the applied ultrasound and powered the sensor. The relaxation oscillator temperature sensor modulated the impedance across the piezoelectric transducer, leading to vibration at the sensor's temperature dependent oscillation frequency, which could be wirelessly read out by the ultrasonic imager.

The application of long-term, real-time temperature monitoring can aid our understanding of disease mechanisms and facilitate early detection and intervention of diseases. In the study by Madhvapathy et al., researchers developed a miniaturized, wireless, implantable sensor designed for the longitudinal monitoring of intestinal temperatures, aiming to facilitate early detection and ongoing management of inflammatory bowel diseases, specifically Crohn's disease[93]. The sensor's architecture comprises a printed circuit board with a Bluetooth low-energy system-on-chip, including an integrated temperature sensor powered by a coin cell battery. This assembly is encapsulated within a polyolefin coating to ensure biocompatibility and durability for long-term implantation. Through in vivo experimentation in a mouse model exhibiting Crohn's-disease-like ileitis, the device demonstrated its capability to record temperature variations within the intestine over several months. Notably, the sensor identified specific patterns of temperature fluctuations—termed ultradian rhythms—that correlated with the onset of inflammation well before the appearance of visible intestinal lesions characteristic of Crohn's disease. This correlation suggests the potential of temperature monitoring as a predictive tool for disease progression. Additionally, the study observed a relationship between these temperature patterns and systemic biological markers, including serum levels of pro-inflammatory cytokines and stress hormones, providing a multidimensional view of the

View Article Online
DOI: 10.1039/D4TB00782D

disease state. These findings highlight the sensor's potential utility in early disease detection and offer a new approach to managing conditions traditionally reliant on invasive diagnostic methods.

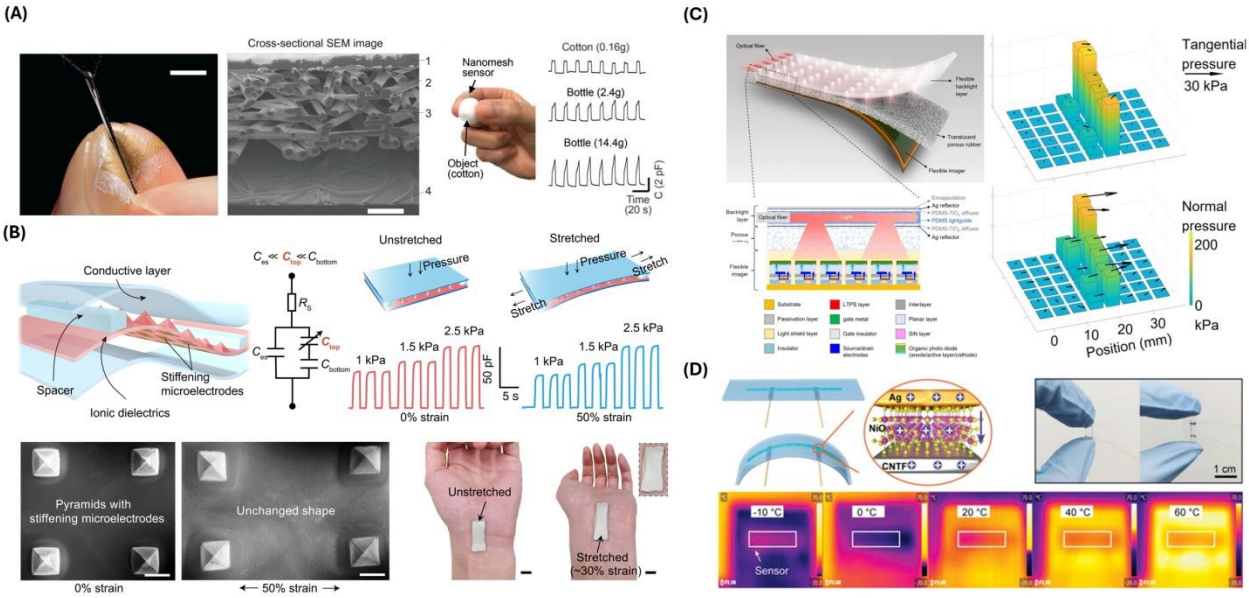

Figure 2. Physical sensing strategies and devices. (A) Photograph of nanomesh pressure sensor attached on finger (left). Scale bar, 5mm. Cross-sectional scanning electron microscopy (SEM) image of the nanomesh sensor on polyimide film (middle). Subject wearing nanomesh sensor to measure grip force of grasping cotton ball (right). Capacitance as a function of time when subject grasps a cotton ball vs. plastic bottles. Reproduced from reference 78 with permission from *AAAS*, copyright 2020. **(B)** Structure and performance of the stretchable pressure sensor. SEM images and photographs of the pressure sensor are shown under stretched vs. unstretched conditions. Reproduced from reference 79 with permission from *AAAS*, copyright 2021. **(C)** Illustration of the Optical-based multipoint 3-axis pressure sensor and cross-sectional view of the sensor structure. Representative data shows multipoint 3-axis pressure distribution detection. Reproduced from reference 82 with permission from *AAAS*, copyright 2023. **(D)** Schematics of the NiO/CNTF flexible temperature sensor. Electrical and temperature sensing characteristics are shown. Reproduced from reference 84 with permission from *Advanced Materials*, copyright 2024.

2.3 Electrophysiological Sensing

Electrophysiological biosensing represents a critical facet in the monitoring and analysis of the body's inherent electrical activities. It encompasses a wide range of applications, from clinical diagnostics to personalized health tracking. This domain is broadly categorized into invasive and surface sensing techniques, each catering to distinct requisites and applications.

Invasive electrophysiological sensing involves direct contact with the target neural or muscular sites through surgical procedures. Techniques like intracranial electroencephalography (EEG) use

View Article Online
DOI: 10.1039/D4TB00782D

electrodes implanted on or within the brain to monitor electrical activities. This approach is crucial for identifying epileptogenic zones and guiding surgical interventions, which offers detailed insights into brain functions [94] . One novel invasive electrophysiological device was developed by Yang et al [95]. The study introduces neuron-like electronics (NeuE) to mimic neurons' structural and mechanical properties, addressing disparities between neural probes and neuron targets that disrupt native tissue and impair neural interfacing stability. NeuE fabrication involves photolithography to create metal recording electrodes. It interconnects within a thin polymer layer to emulate the size and flexibility of pyramidal neuron components, thereby significantly reducing mechanical stiffness compared to existing probes and matching subcellular neuronal component flexibility. The NeuE design's novelty lies in its three-dimensional electronic network, which mirrors neural network topology and improves integration with brain tissue. The NeuE probe can record chronic neural activity over three months and capture single-unit spikes with stable signal-to-noise ratios and electrode impedances.

Woodington et al. present a novel thin-film, flexible electronic device designed for comprehensive interfacing with the spinal cord[96]. The sensing mechanism of this device is based on a sophisticated electrode configuration featuring a thin, flexible electrode array with 32 electrodes arranged in a staggered, linear layout (Fig. 3A). This configuration maximizes the circumferential distribution of electrodes around the spinal cord while minimizing crosstalk contamination. The electrodes, made from titanium and gold and coated with PEDOT:PSS, reduce impedance, enhancing both recording and stimulation performance. Using electrical impedance spectroscopy, the device records neural signals from various spinal cord tracts. The recorded signals create topographic maps of neural activity to facilitate detailed representations of the spinal cord's neural functions (Fig. 3B). Targeted electrical stimulation is achieved through electrodes, which activate motor neurons and elicit controlled muscle movements, with the PEDOT coating enhancing charge storage and injection capacity for safe stimulation. The design allows for precise, localized stimulation, selectively activating specific motor groups without affecting adjacent areas. Functioning in a closed-loop system, the device uses recorded neural signals to trigger stimulation, bypassing damaged

View Article Online
DOI: 10.1039/D4TB00782D

spinal cord regions to restore motor functions. Key characteristics monitored include neural signal amplitude and spatial distribution, enabling motor and sensory signal integrity measurement. When irregularities are detected, targeted stimulation is applied to restore function. The control module processes signals, triggering appropriate responses to maintain or restore motor functions in a closed-loop system. The logical flow diagram involves continuous signal recording, real-time processing and analysis, automatic detection of irregularities, and immediate stimulation response to bypass damaged neural pathways. This integrated approach highlights the potential for significant advancements in therapeutic interventions for spinal cord injuries and related neurological disorders, making it a powerful tool for spinal cord injury research and potential clinical applications.

Surface sensors adopt a non-invasive approach and are important in the interface of electrophysiological organs and wearable technology. These sensors are designed to comfortably capture signals like electrocardiograms (ECG), electromyograms (EMG), and EEG over long periods. Wearable and stretchable electrophysiological sensing devices are categorized primarily into piezoresistive, piezoelectric, iontronic, and capacitive sensors[97]. Each leverages unique principles to transduce physiological signals into electrical outputs. Piezoresistive sensors rely on the variation of electrical resistance under mechanical deformation, making them ideal for capturing strain or pressure changes[98, 99]. They are often constructed from materials such as silicon, which exhibit a change in resistance when stressed, directly measuring mechanical forces. Piezoelectric sensors harness materials that generate an electrical charge in response to mechanical stress[100]. This effect, found in materials like polyvinylidene fluoride, allows for the direct conversion of mechanical movements into electrical signals and is suitable for monitoring dynamic physiological activities like heart rate and vocal cord vibrations. Iontronic sensors represent a novel category, focusing on the interactions between ionic and electronic charges[101, 102]. Utilizing ionic gels or electrolytes, these sensors excel in environments rich in ionic content, such as human sweat, enabling the measurement of ionic flux or concentration changes. Capacitive sensors, recognized for their high sensitivity and non-invasive nature, measure changes in capacitance resulting from the dielectric

View Article Online
DOI: 10.1039/D4TB00782D

properties of biological tissues or the proximity between the sensor and the skin[103, 104]. Flexible substrates and conductive coatings are critical to their design, allowing for a wide range of health monitoring applications, from heart rate to gesture recognition.

Zhou et al. present a system using soft and stretchable organic-electronic materials for continuous intraoperative neurophysiological monitoring in microneurosurgery[105]. This system employs conducting polymer electrodes, specifically PEDOT:PSS, optimized for low impedance and flexibility to record near-field action potentials. These features allow for superior signal-to-noise ratios and reduced invasiveness compared to conventional clinical probes. Their study shows that these electrodes, when wrapped around the trigeminal nerve (CN V), facial-acoustic nerve complex (CN VII, CN VIII), and lower cranial nerves (CN IX-XI), enable precise nerve localization and record cochlear nerve action potentials with minimal invasiveness, significantly enhancing post-operative outcomes in rat models (Fig. 3C). The fabrication process involves blending PEDOT with a crosslinkable supramolecular additive to produce electrodes that are both conductive and stretchable. This method ensures that the electrodes conform closely to nerve structures, reducing mechanical mismatches and improving signal quality. Zhou et al.'s findings demonstrate the system's efficacy in recording cochlear nerve action potentials with minimal invasiveness during surgery.

Fang et al. introduced a novel cardiac monitoring system using capacitively coupled arrays of multiplexed flexible silicon transistors[106]. This system employs an ultrathin, biocompatible dielectric layer to encapsulate the electronics, thus protecting them from biological fluids and electrochemical degradation. This design allows for electrophysiological measurements through capacitive coupling and eliminates the need for direct metal contact. It significantly reduces leakage levels and extends operational lifetimes beyond current technologies. The core innovation lies in the capacitive coupling facilitated by the silicon dioxide layer, which acts as a dielectric for signal measurement and a barrier against bio-fluid penetration. This dual function ensures a robust, noninvasive, high-fidelity cardiac signal capture interface. The fabrication process utilizes semiconductor techniques to create thin, flexible electronics capable of

View Article Online
DOI: 10.1039/D4TB00782D

conforming to the dynamic surfaces of biological tissues. This method enables the production of extensive and high-density sensor arrays for comprehensive cardiac mapping on beating hearts. Fang et al. illustrate the system's capacity to map electrophysiological activities under various cardiac conditions, such as normal rhythms, paced rhythms, and arrhythmias in ex vivo heart models. This capability shows the system's utility for both clinical diagnostics and research.

One comprehensive closed-loop system that utilizes surface sensors was introduced by Yeon Sik Choi et al.[107]. This system presents a transformative approach to autonomous electrotherapy by integrating a bioresorbable epicardial pacemaker with a sophisticated array of skin-interfaced sensors. The sensing mechanism in this system involves a combination of these sensors and the pacemaker to monitor physiological characteristics. The skin-interfaced sensors include a cardiac module with an ECG sensor that captures the heart's electrical activity to monitor heart rate and detect arrhythmias, an analog front end for processing raw ECG signals, a microcontroller unit for real-time analysis of ECG data to calculate heart rate and detect anomalies, and Bluetooth communication for data transmission to the control module (Fig. 3D). The respiratory module, mounted at the suprasternal notch, uses a dual-sensing design to measure physical activity, body temperature, and respiratory behavior, providing insights into respiratory health. The hemodynamic module on the forehead employs a pulse oximetry sensor to measure peripheral blood oxygen saturation (SpO2). Additionally, the multihaptic module, located on the mid-medial forearm, provides up to 625 patterns of mechanical vibrations to communicate patient status and device operation, informing the patient about system status, remaining battery life, and device functionality. The bioresorbable epicardial pacemaker includes a wireless power harvester with an inductive receiver coil that captures wireless power transmitted by the skin-interfaced RF module and a PIN diode that rectifies the received alternating current (AC) into direct current (DC) to power the pacemaker. It also features stimulation electrodes that deliver pacing pulses to the heart and a steroid-eluting interface that releases anti-inflammatory agents to minimize local inflammation and fibrosis. The control module, a handheld device with a software application, facilitates real-time data visualization, storage, and analysis, enabling

View Article Online
DOI: 10.1039/D4TB00782D

algorithmic control for adaptive pacing decisions. The closed-loop control system employs hysteresis pacing, delivering programmed electrical stimuli when the intrinsic heart rate falls below a set threshold. This feedback mechanism evaluates the need for pacing based on real-time physiological data and adjusts treatment accordingly. The logical flow diagram of the closed-loop system involves continuous monitoring, detection of physiological anomalies, autonomous initiation of therapy, and feedback provision via a multihaptic interface.

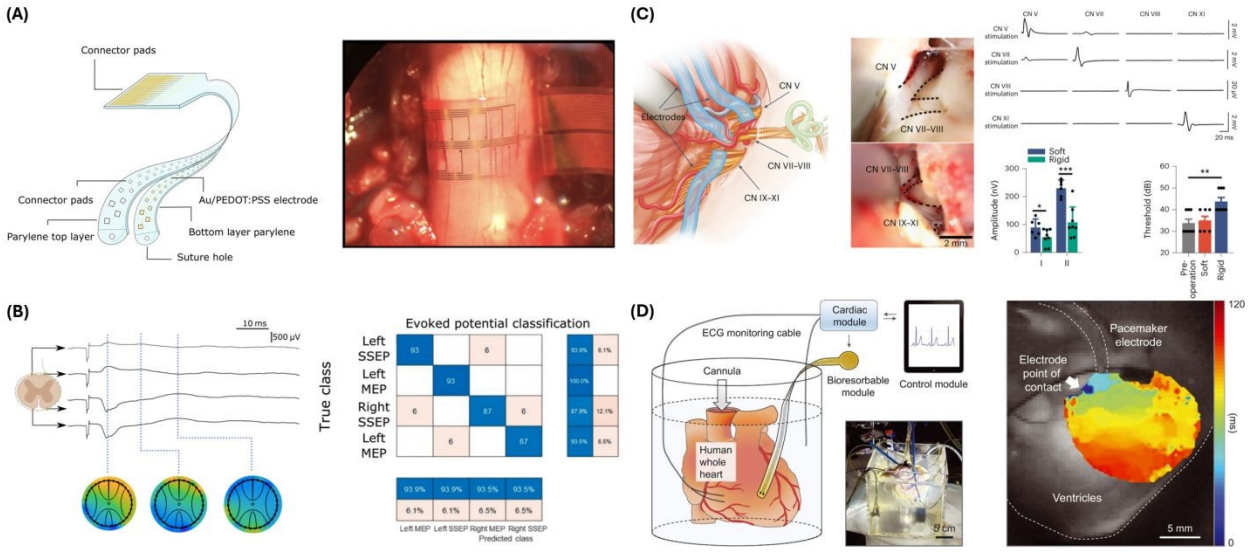

Figure 3. Electrophysiological sensing strategies and devices. **(A)** Illustration of the microfabricated I360 device design (left) and an intraoperative photograph showing the device wrapped around the spinal cord above the L1 superior facet (right). Reproduced from reference 96 with permission from *AAAS* under terms of the Creative Commons CC BY license, copyright 2024. **(B)** Diagram showing I360 device recorded signals over time following sciatic nerve stimulation (left). Matrix classification shows positive and negative hit rates of stimulation events. Reproduced from reference 96 with permission from *AAAS* under terms of the Creative Commons CC BY license, copyright 2024. **(C)** Flexible PEDOT electrodes are used for conformable neural interfaces and functional characterization when recording CN V, CN VII, CN VIII, and CN XI nerves. Soft vs. rigid electrode functional characterizations show minimal invasiveness of the soft PEDOT electrodes. Reproduced from reference 105 with permission from the copyright owner and *Springer Nature*, © 2023. **(D)** Schematic illustration and photograph of a Langendorff-perfused human heart model with a transient closed-loop system (left). Action potential mapping of the human epicardium (right). Reproduced from reference 107 with permission from *AAAS*, copyright 2022.

Table 1. Classification of Sensors

Sensor Type	Mechanism	Aims/Characteristics	Application in Closed-Loop Systems
Chemical Sensors	Redox-based, impedance-based, transistor-based, and pH-responsive	Detect biomarkers and metabolic parameters, continuous tracking, specificity and	Real-time monitoring of biomarkers, enabling adaptive drug delivery and metabolic

View Article Online
DOI: 10.1039/D4TB00782D

		sensitivity, integration with microfluidic systems.	monitoring. Essential for chronic disease management.
Physical Sensors	Pressure and temperature sensing (capacitive, piezoelectric, thermal resistive, thermoelectric, frequency output)	High sensitivity, flexibility, rapid response, strain-insensitivity, mechanical durability.	Monitoring signs such as blood pressure, intraocular pressure, intracranial pressure, and temperature; enhancing therapeutic interventions.
Electrophysiological Sensors	Invasive (intracranial, spinal cord) and surface (wearable, stretchable)	Capture electrical activities of neural and muscular systems, flexible, biocompatible, high signal-to-noise ratio.	Monitoring and stimulating neural activities, restoring motor functions, managing heart rhythms, and providing sensory feedback.

3.1. Drug Delivery

Devices to improve current drug delivery methods have been developed for various applications. Recent general approaches center around the use of microneedles, implantables, and ingestibles as drug delivery platforms (Table 2). This section presents the details of each modality.

3.1.1. Microneedle Delivery

Conventional needle injections are considered invasive, and as a result, methods like transdermal drug delivery systems (TDDS) have been developed. Since providing a less invasive drug delivery approach that can maximize therapeutic efficacy while minimizing side effects, TDDS has been a compelling approach [108]. One of the most common categories of TDDS is microneedle (MN) drug delivery.

A self-plugging MN has been developed for intravitreal drug delivery[109]. Intravitreal injection is a type of intraocular drug administration procedure where drugs are directly injected into the vitreous cavity inside the eye to treat ophthalmic diseases via hypodermic needles. This often results in patients suffering adverse effects such as intraocular inflammation, pain, blurred vision, and other ocular side effects[110-112]. These effects may be attributed to the fact that when hypodermic needles are extracted after being inserted into the vitreous cavity to treat diseases like retinoblastoma, tumor cells from the vitreous cavity may escape via the puncture hole incurred by the hypodermic needles, thereby leaving the eye susceptible to becoming

View Article Online
DOI: 10.1039/D4TB00782D

infection[113-115]. Lee et al. introduced an MN coated with a polymeric drug carrier, which exhibits a gradual release effect inside eyeball[109]. To tackle the problem of a lack of a sealant for the puncture incision from hypodermic needles, the MN developed a biocompatible swelling hydrogel coating to provide a self-plugging or clogging effect. In vitro and ex vivo experiments were performed to show the functionalized coating layer on the MN, and in vivo tests using a porcine model verified the sealing effect's promptness and sustained intraocular drug delivery capabilities.

MN patches are a common way of utilizing MN for therapeutic benefits. Fang et al. have developed a porous MN patch for sustained delivery of extracellular vehicles (EVs) to mitigate severe spinal cord injury (SCI)[116]. Because SCI lesions trigger neuroinflammatory microenvironments detrimental to the survival and function of mesenchymal stem cells (MSCs), MSCs secreted extracellular vesicles (MSC-EVs) enabled the therapeutic effect of this treatment method [117-119]. The methods involve fabricating a porous GelMa hydrogel MN, loading MSCs onto the basal side of the MN arrays, and conducting a 30-s blue light curing process to obtain the EV-secreting porous MN-MSC patch. The device was tested in vivo using a rat SCI model. It demonstrated its ability to induce drastic functional recovery by reducing cavity and scar tissue formation, alleviating neuroinflammation triggered by SCI, promoting angiogenesis, and improving the survival of nearby tissue and axons. Through harnessing the MSC-EVs' therapeutic effects, this study avoids direct invasion of MSCs into the spinal cord microenvironment. Moreover, the nature of the MN-MSC patches seeded with EVs significantly improved its sustained delivery capacity, which lasted for at least seven days, exceeding that of both direct injections of MSCs and direct infusion of MSC-EVs. Zhu et al. introduced a wet-bonding MN patch, inspired by the blue-ringed octopus, composed of silk fibroin-Pluronic F127 (Silk-Fp), which allows for tissue adhesion and effective topical medication[120]. The patch also includes a hydrogel-based flexible suction cup that enables biocompatible chemical bonding and physical adhesion due to air pressure difference and protects the inner chemical bonding interface against liquid environments [121, 122]. Since the Silk-Fp patch developed has physical/chemical joint-bonding abilities, it can resist wet tissue and keep its stability for days while carrying out a controllable drug-releasing effect. The Silk-Fp patches were tested for their therapeutic effects on oral ulcers in rabbits. The patch was found

View Article Online
DOI: 10.1039/D4TB00782D

to decrease the ulcer's size and shorten the hearing process time. The Silk-Fp patch's therapeutic effects on early melanoma in mice were also examined. The Silk-Fp could suppress early tumors' growth, though it regulated late melanoma growth at a deficient level. Specifically, results show that tumor sizes were noticeably smaller compared to other groups tested, being 5% the weight of the blank tumor group and that the patch had therapeutic effects lasting more than ten days.

A wearable MN-based array patch enabling continuous electrochemical monitoring and drug delivery has been developed by Parrilla et al[123]. The patch had MN-based electrochemical sensors for transdermal monitoring of the interstitial fluid and delivery of methotrexate (MTX), a chemotherapy and immunosuppressive drug. The sensor component of the device was examined through ex vivo experiments in porcine skin to demonstrate its ability to monitor MTX concentrations. On top of the sensor component, with an MTX-containing hydrogel loaded into the patch reservoir, an on-demand iontophoretic hollow microneedle array system was used to provide a current that would influence the migration of MTX for drug delivery effects. As such, this device presents a self-sufficient management of MTX therapy, which may be used for cancer patients, encompassing a closed-loop sensing and drug delivery system.

Nonetheless, despite numerous advancements in MN drug delivery devices, there are few developments in incorporating a closed-loop component. Many MN drug delivery systems can benefit from incorporating an on-demand control built into MN patches, giving it a closed-loop ability. Yang et al. detail developing a transdermal microneedle patch for closed-loop insulin and glucagon delivery to manage diabetes in mouse and pig models through dynamic adjustment to blood glucose levels[124]. The glucose-responsive microneedle (GRD-MN) patches, fabricated via photopolymerization, incorporate phenylboronic acid units that react to glucose concentration changes by altering the patch's charge, thus controlling the release of insulin and glucagon (Fig. 4A). This mechanism enables the patch to release insulin during hyperglycemia and glucagon during hypoglycemia, closely mimicking the natural glucose regulation of the pancreas. In vivo, the patch's efficacy was validated through its application to diabetic mice, demonstrating its ability to penetrate the skin without causing significant damage or inflammation. The study's results indicated that diabetic mice treated with the GRD-MN patch maintained normoglycemia

View Article Online
DOI: 10.1039/D4TB00782D

for extended periods without experiencing hypoglycemia, unlike mice treated with insulin-only patches (Fig. 4A). Moreover, the patch was tested in a diabetic minipig model, where it successfully managed glucose levels over 24 hours, demonstrating its effectiveness in a model closely resembling human physiology.

Abramson et al. developed an ingestible capsule, termed the luminal unfolding microneedle injector (LUMI), designed to enhance the oral delivery of biological drugs like insulin[125]. This innovative device propels dissolvable drug-loaded microneedles into intestinal tissue using unfolding arms to overcome the challenge of macromolecule absorption through the gastrointestinal tract. Fabrication of the LUMI capsule involved a meticulous design process to optimize contact with intestinal tissue and ensure safe deployment and dissolution. The capsule is coated with a material that dissolves at specific pH levels, ensuring release in the small intestine. It houses a compressed spring mechanism that propels the LUMI device out of the capsule. The LUMI device comprises three degradable arms loaded with 1-mm-long, dissolvable microneedles containing the drug. The arms are designed to stretch the intestinal tissue slightly, ensuring microneedle penetration without perforation. In vitro and in vivo studies in swine demonstrated the LUMI's ability to consistently deliver microneedles to the tissue, showing faster pharmacokinetic profiles and over 10% systemic uptake for insulin compared to subcutaneous injections. These promising results indicate the LUMI's potential as a versatile platform for the oral delivery of various macromolecule drugs.

3.1.2. Implantable Delivery

Implantable drug delivery systems integrated with biosensing capabilities allow for the real-time monitoring of physiological parameters and the delivery of therapeutic agents in response to specific biomarkers or health conditions. This approach optimizes therapeutic outcomes by ensuring drugs are released at the right time and in the correct doses[126].

Sung et al. introduced a flexible drug delivery microdevice designed for controlled administration via implantation in the curved cerebral cortex[127]. Key to the device's functionality is its unique assembly process, which inverts the conventional order of fabricating the reservoir and sealing layers. This process begins with the deposition of a hydrogenated amorphous silicon (a-Si:H) layer and a subsequent SiO2 buffer

View Article Online
DOI: 10.1039/D4TB00782D

layer via plasma-enhanced chemical vapor deposition on a rigid substrate. Metal electrodes composed of a Ti/Au/Ti stack are then patterned atop this foundation. The multi-reservoir array is structured using SU-8 photoresist and filled with therapeutic agents before sealing it with the gold membrane. This membrane is the electrode for electrical input and a barrier to premature drug release. Electrochemical dissolution of the gold membrane, triggered by an external electric bias, allows for controlled release of the encapsulated drugs. This process is tuned by applying a constant current density and optimized based on in vitro electrochemical analysis. This ensures reliable release kinetics without inducing thermal or chemical damage to the stored drugs or surrounding tissue. The application of a wireless power transfer system further enhances the device's utility by eliminating the need for direct electrical connections, thus facilitating its use in vivo. The device is said to be capable of treating central nervous system disorders like epilepsy, Parkinson's disease, and Huntington's disease.

An innovative implantable device designed by Koo et al. enables precise, programmable drug release and complete bioresorption post-treatment [128]. The sensing mechanism relies not on traditional sensors but on external wireless signals to sense and trigger drug release. The device is equipped with an RF coil that wirelessly harvests power from an external RF transmission source, coupled with an RF diode and a capacitor forming a resonant circuit tuned to approximately 5 MHz, ensuring efficient power transfer with minimal absorption by biological tissues (Fig. 4B). The control mechanism is electrochemical, where an applied RF signal induces an electrical current in the RF coil, creating a voltage bias between magnesium electrodes, triggering an electrochemical reaction at the anode. This reaction accelerates corrosion at the interface between the anode gate and the surrounding polyanhydride (PBTPA) housing, known as crevice corrosion. This geometrically accelerated corrosion rapidly and efficiently dissolves the metal gate, opening the drug-containing reservoir. The drug release is thus controlled by the design and dimensions of the gate and the applied electrical bias. Key components include the RF coil for power harvesting, RF diode and capacitor for resonance, magnesium electrodes for the electrochemical reaction, and PBTPA housing for drug containment. The monitored characteristics include the gate's integrity and drug release timing, which are controlled via external RF signals. The RF control can adjust the system upon encountering issues such

View Article Online
DOI: 10.1039/D4TB00782D

as premature release or failure to release. The logic of this system encompasses power harvesting, electrochemical triggering, gate corrosion, and drug release, forming a robust, self-contained mechanism for targeted drug delivery (Fig. 4B). This integration of wireless power transmission and electrochemical control offers a sophisticated solution for controlled, localized pharmacological treatments. The system enables real-time monitoring and responsive treatment adjustments, essential for effectively managing conditions requiring precise drug dosing.

Another example of an integrated implantable drug delivery system was designed by Zhang et al. [129]. This platform employs phototransistors paired with optical filters to sense specific wavelengths of light, triggering the corrosion of bioresorbable metal gates and releasing drugs from reservoirs in a controlled manner. The use of bioresorbable materials such as magnesium (Mg), magnesium coated with spin-on glass (Mg-SOG), and polyanhydride (PA) ensures the device naturally dissolves in the body, reducing the need for surgical removal. In vivo studies demonstrate effective pain management in rat models, underscoring the potential clinical applications of this technology. The device monitors the illumination of phototransistors to determine which drug reservoir to activate, allowing for precise control over the timing and sequence of drug release events. If a reservoir fails to open or release the drug correctly, the external light source can be recalibrated or adjusted to ensure proper activation of the phototransistor. The control module comprises an external light source, such as LEDs, programmed to emit specific wavelengths of light and responsible for sending signals to the phototransistors to initiate the drug release process. This module also includes the software and hardware necessary for programming and adjusting the light signals. The process begins with activating the external light source, which illuminates the phototransistor, causing a decrease in its resistance and creating a short circuit in the electrochemical cell. This short circuit accelerates the corrosion of the bioresorbable metal gate, opening the drug reservoir and releasing the drug into the surrounding tissue. This logical flow from light activation to drug release ensures a highly controlled and precise drug delivery mechanism, presenting a promising solution for enhancing patient care and treatment outcomes.

3.1.3. Ingestible Delivery

View Article Online
DOI: 10.1039/D4TB00782D

The gastrointestinal (GI) tract serves as a conduit for detecting physiological and pathophysiological signals within the human body. Ingestible electronics that navigate the GI tract present a promising avenue for clinical applications in diagnostics and therapy[130]. Specifically, they offer targeted drug delivery solutions, which are particularly advantageous for addressing gastrointestinal conditions.

For example, The IntelliCap® system is an ingestible capsule designed for precise drug delivery within the GI tract, equipped with pH and temperature sensors, a microprocessor, a wireless transceiver, and a stepper motor-driven drug reservoir[131]The system's core mechanism involves a microprocessor-controlled stepper motor. This motor actuates a plunger to expel the drug payload at preprogrammed rates, directly correlating in vivo release with in vitro-designed profiles through deconvolution analysis. A clinical trial using metoprolol validated the system's capability for accurately mimicking intended release kinetics, particularly for linear profiles. However, challenges in delivering the second pulse of a pulsed release profile in the distal GI tract indicated limitations in the system's performance in varying GI environments.

The development of RoboCap by Srinivasan et al. presents a groundbreaking solution to the longstanding challenges of oral drug delivery, particularly for proteins within the gastrointestinal tract[132]. This innovation addresses the crucial issue of poor absorption and degradation in the harsh gastrointestinal environment, which has historically necessitated parenteral administration for many drugs[133]. By locally clearing the mucus layer, enhancing luminal mixing, and precisely depositing the drug payload in the small intestine, RoboCap demonstrates remarkable potential to improve drug absorption significantly. Incorporating surface features that interact with intestinal structures and mucus, facilitating rotational and churning movements, is particularly ingenious. The observed 20- to 40-fold increase in bioavailability of vancomycin and insulin compared to standard oral delivery in both ex vivo and in vivo swine models demonstrates the impact of this technology. The RoboCap represents an advancement in oral drug delivery, offering a new avenue for enhancing therapeutic outcomes and expanding treatment options for a wide range of drugs previously hindered by absorption limitations.

Zheng et al. introduce a multifunctional capsule robot (MCR) designed for active locomotion, dual-drug loading, and selective drug release to address limitations in robot-assisted drug delivery for intestinal

View Article Online
DOI: 10.1039/D4TB00782D

diseases[134]. The MCR achieves a high ratio of drug volume to total capsule volume (RDC) and can deliver sufficient dosages for treatment. Controlled by two orthogonal rotating magnetic fields, the MCR consists of locomotion and drug delivery units, allowing it to target positions and release two drugs as needed. In vitro and ex vivo experiments demonstrate the MCR's capabilities, including a maximum drug loading capacity of 1.5 g, advance and retreat velocities of up to 11.8 mm/s and 10.4 mm/s, respectively, when fully loaded, and successful drug release without visible damage to the intestine. This innovation can improve intestinal disease treatment by reducing costs and enhancing treatment efficiency through dual-drug delivery and high RDC. Additionally, developing a dual-drug release mechanism and a control method enhances the MCR's adaptability and reliability in complex environments.

Abramson et al. developed an innovative ingestible self-orienting millimeter-scale applicator (SOMA) inspired by the leopard tortoise's ability to self-orient for the oral delivery of macromolecules like insulin[135]. This device autonomously positions itself to engage with gastrointestinal tissue correctly, then deploys drug-loaded "milliposts" directly through the gastric mucosa without perforation, aiming to achieve systemic drug uptake levels comparable to subcutaneous administration (Fig. 4C). The SOMA's design and fabrication involve a monostatic body optimized for rapid self-orientation and stability against external forces. The device utilizes a combination of low-density poly(caprolactone) and high-density stainless steel to achieve a low center of mass necessary for self-orientation. The drug-loaded milliposts, fabricated from a high-pressure mixture of insulin and biodegradable polymers, are designed to dissolve within the gastric environment, releasing the active pharmaceutical ingredient. In vivo studies conducted on rats and swine demonstrated the safety of the device and its efficacy in delivering insulin. Pharmacokinetic and systemic uptake results from the application of this device were comparable to those achieved with manual subcutaneous injections of the milliposts.

View Article Online
DOI: 10.1039/D4TB00782D

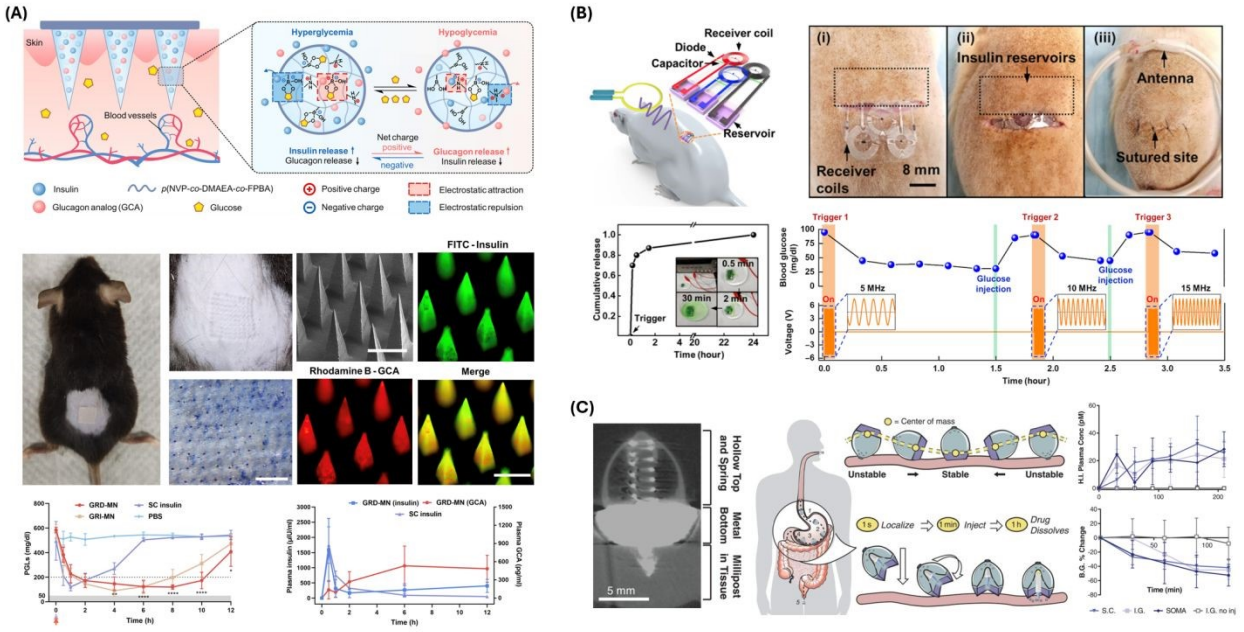

Figure 4. Drug delivery approaches and devices. (A) Schematic, fabrication process, and characterization of the GRD-MN patch. In vivo assessment of the GRD-MN patch in live streptozotocin-induced diabetic mouse models is shown. GRI-MN, glucose-responsive insulin-only MN; SC, subcutaneous. Reproduced from reference 124 with permission from *AAAS*, copyright 2022. **(B)** Wirelessly controlled, bioresorbable drug delivery device with electrochemically triggered crevice corrosion valves. Graph shows blood glucose level changes induced by insulin release from the three independent reservoirs. RF with different frequencies (5, 10, and 15 MHz) triggered each reservoir. Reproduced from reference 128 with permission from *AAAS*, copyright 2020. **(C)** Micro-CT image of SOMA administering barium sulfate millipost to swine stomach tissue (left). Schematics illustration SOMA localization and drug injection after oral delivery. In vivo human insulin delivery and device assessment in swine model. Reproduced from reference 135 with permission from *AAAS*, copyright 2019.

Table 2. Drug Delivery Systems

Drug Delivery Type	Representative Designs	Aims/Characteristics	Application in Closed-Loop Systems
Microneedle Delivery	Transdermal patches, polymeric coatings, porous structures, glucose-responsive mechanisms	Minimally invasive, sustained release, enhanced therapeutic efficacy, real-time response to physiological changes	Diabetes management (glucose-responsive insulin delivery), spinal cord injury treatment, sustained medication release
Implantable Delivery	Wireless control, electrochemical triggers, bioresorbable materials, phototransistors	Precision drug release, real-time monitoring, complete bioresorption, programmable and controlled	Treatment of neurological conditions (epilepsy, Parkinson's), pain management, programmable drug delivery
Ingestible Delivery	pH and temperature sensors, magnetic control, dual-drug loading mechanisms	Targeted drug release in the gastrointestinal tract, variable drug volume capacity,	Treatment of gastrointestinal diseases, oral delivery of biologics, dual-drug

View Article Online
DOI: 10.1039/D4TB00782D

		enhanced bioavailability	therapy for complex conditions

3.2 Electrical Stimulation

Electrical stimulation involves applying controlled electrical currents or potentials to biological tissues, eliciting specific responses that can be quantified via biosensors. Table 3 summarizes electrical stimulation devices, their mechanisms, key characteristics, and applications in closed-loop therapeutic systems. Bioelectronic medicine is advancing rapidly, aiming to alleviate clinical conditions by stimulating the peripheral nervous system (PNS) with electrical methods. A study explored the impact of electrical stimulation on motor axonal regeneration in the PNS, evaluating its effects on the speed of axonal regeneration, the reinnervation of appropriate muscle pathways, and the underlying mechanism of action. Al-Majed et al. applied retrograde neurotracers to label motoneurons and assessed the effects of various durations of electrical stimulation [136]. The study found that axonal outgrowth, typically prolonged over ten weeks, was significantly reduced to 3 weeks with short-term electrical stimulation (1 hour to 2 weeks) at 20 Hz. This stimulation accelerated axonal regeneration and promoted preferential motor reinnervation (PMR), mediated via the cell body, suggesting an enhanced growth program. The clinical implications are significant, indicating that short-term, low-frequency electrical stimulation could be a viable therapeutic approach to accelerate nerve regeneration and improve functional recovery after nerve injuries.

These advancements in electrical stimulation underscore the potential for innovative approaches in bioelectronic medicine. Jiang et al. introduced a novel approach to the design of electrophysiological sensors by integrating a topological supramolecular network into the architecture of bioelectronic interfaces (Fig. 5A)[137]. It utilizes a cross-linkable supramolecular additive known as TopoE, which is based on a polyrotaxane (PR) structure. The PR structure enhances both the conductivity and stretchability of conducting polymers, essential attributes for the development of bioelectronic devices capable of seamless integration with physiological environments. This topological supramolecular network is based on a polyethylene glycol (PEG) backbone adorned with sliding cyclodextrins (CDs) functionalized with PEG

View Article Online
DOI: 10.1039/D4TB00782D

methacrylate (PEGMA) side chains. This configuration mitigates the risk of PEG crystallization, thereby preserving the material's stretchability and significantly boosting the conductivity of PEDOT:PSS films. It accomplishes this by facilitating the removal of insulating polystyrene sulfonate when the material is immersed in aqueous environments. Jiang et al. demonstrated the application of their material in capturing stable electromyography signals from soft tissues. More notably, the study shows the capability of these materials to achieve localized neuromodulation with single-nucleus precision within the brainstem (Fig. 5A). This level of specificity and integration highlights the potential of Jiang et al.'s topological supramolecular network in electrophysiological applications.

Wu et al. have developed a self-powered electronic bandage using soft and biodegradable materials to accelerate intestinal wound healing[138]. Intestinal wound healing presents challenges due to the intricate structure and microenvironment of the intestinal tract[139, 140]. To address this, a self-powered electronic bandage (E-bandage) has been developed, integrating dual electrostimulation mechanisms to address intestinal wound healing challenges. Constructed from flexible, biocompatible, and biodegradable materials, the E-bandage incorporates magnesium and molybdenum microelectrodes and a tissue-adhesive hydrogel with DNA plasmids. Pulsed electrostimulation induces electrotransfection of epithelial cells, enhancing the expression of healing factors such as epithelial growth factors (EGFs), while d.c. electrostimulation boosts the secretion of these factors. Additionally, the bandage's self-powered galvanic cell promotes healing factor exocytosis. The E-bandage facilitates increased EGF expression by demonstrating high transfection efficiency and cell viability in vitro. In vivo mouse models attest to their efficacy in promoting EGF generation, fostering the proliferation of intestinal tissue layers and augmenting probiotic populations. Compared to conventional sutures, the E-bandage mitigates postoperative complications and accelerates body weight recovery. As such, this study presents a promising approach to expediting intestinal wound healing by developing a self-powered electronic bandage with dual electrical stimulation capabilities.

View Article Online
DOI: 10.1039/D4TB00782D

A bioresorbable peripheral nerve stimulator developed by Lee et al. employs a mechanism that allows for electrical nerve block to manage pain without pharmacological agents [141]. This system provides localized electrical stimulation to peripheral nerves, blocking the propagation of action potentials and mitigating pain (Fig. 5B). The device uses kilohertz-frequency alternating current (KHFAC) stimulation, maintaining steady-state depolarization in nerve fibers with high frequency (25 to 35 kHz) and amplitude (10 Vpp), preventing pain signals from reaching the brain. Made of bioresorbable materials, the system gradually dissolves in the body, eliminating the need for surgical removal. Key materials include Molybdenum (Mo) for stable, long-term stimulation; Magnesium (Mg) for extension electrodes; Polylactic-co-glycolic acid (PLGA) for structural support; and Polyanhydride (PA) for encapsulation. The stimulator features a woven structure of interleaved Mo and Mg strips for mechanical strength and electrical connectivity, configured in a tripolar arrangement to minimize current spread. The device is powered externally, with adjustable control parameters for optimal nerve block. Designed for controlled dissolution, the extension electrodes (Mg/PA) dissolve first, followed by the nerve cuff (Mo/PLGA), ensuring gradual, safe bioresorption and minimizing tissue damage. Biocompatible materials and in vivo tests show effective nerve conduction block without significant inflammation or damage. The logical flow of this system involves initial stabilization, followed by sequential, controlled bioresorption, minimizing risks and ensuring effective pain management.

Another representative electrical stimulation device was developed by Koo et al., which leverages a combination of bioresorbable materials and wireless power transfer technology to enable sustained neuroregenerative therapy [142]. The mechanism includes a magnesium loop antenna with a poly (lactic-co-glycolic acid) (PLGA) dielectric interlayer to capture RF energy, a radio frequency diode made from doped silicon nanomembrane with Mg electrodes to rectify the RF energy into a DC signal, and a parallel plate capacitor with Mg conducting planes and a silicon dioxide (SiO2) dielectric layer to store and regulate the electrical charge. The stimulator features an electrode and cuff design that wraps around the nerve, delivering electrical impulses directly to the nerve tissue to promote regeneration while ensuring minimal invasiveness and excellent apposition to prevent damage. The materials are designed to degrade safely

View Article Online
DOI: 10.1039/D4TB00782D

within the body over a defined period, aligning with the therapy duration to minimize long-term risks. The control system uses inductive coupling to wirelessly transfer power from an external transmitter to the internal receiver, with power modulation to control the electrical stimulation's intensity, frequency, and duration. The system delivers cathodic, monophasic electrical impulses (200 μs duration, 100-300 mV threshold voltage) generated in response to the modulated RF power. Extensive in vivo testing confirms the safety and effectiveness of the stimulation parameters for nerve regeneration, with biocompatibility and bioresorption validated through histological analysis.

Closed-loop and wireless “smart” bandages based on sensing modalities that accelerate rates of chronic wound healing have been developed[143-145]. Jiang et al. developed a multimodal bandage with real-time physiological monitoring and active intervention capabilities for promoting chronic wound healing via electrical stimulation (Fig. 5C)[144]. The device is a battery-free flexible bioelectronic system with tissue-interfacing tough hydrogel electrodes consisting of an energy-harvesting antenna, microcontroller unit, and components enabling dual-model monitoring of wound impedance and temperature. It integrates a parallel simulation circuit for programmed electrical cues to increase wound healing, thereby introducing a fully closed-loop smart bandage to provide a therapeutic effect. In pre-clinical wound models, the smart bandage demonstrated accelerated wound closure, increased neovascularization, as well as enhanced dermal recovery compared to the control groups (Fig. 5C). This advancement addresses the limitations of existing smart bandage technologies by incorporating both sensing and stimulation capabilities alongside switchable adhesion to prevent secondary damage to delicate wound tissues.

View Article Online
DOI: 10.1039/D4TB00782D

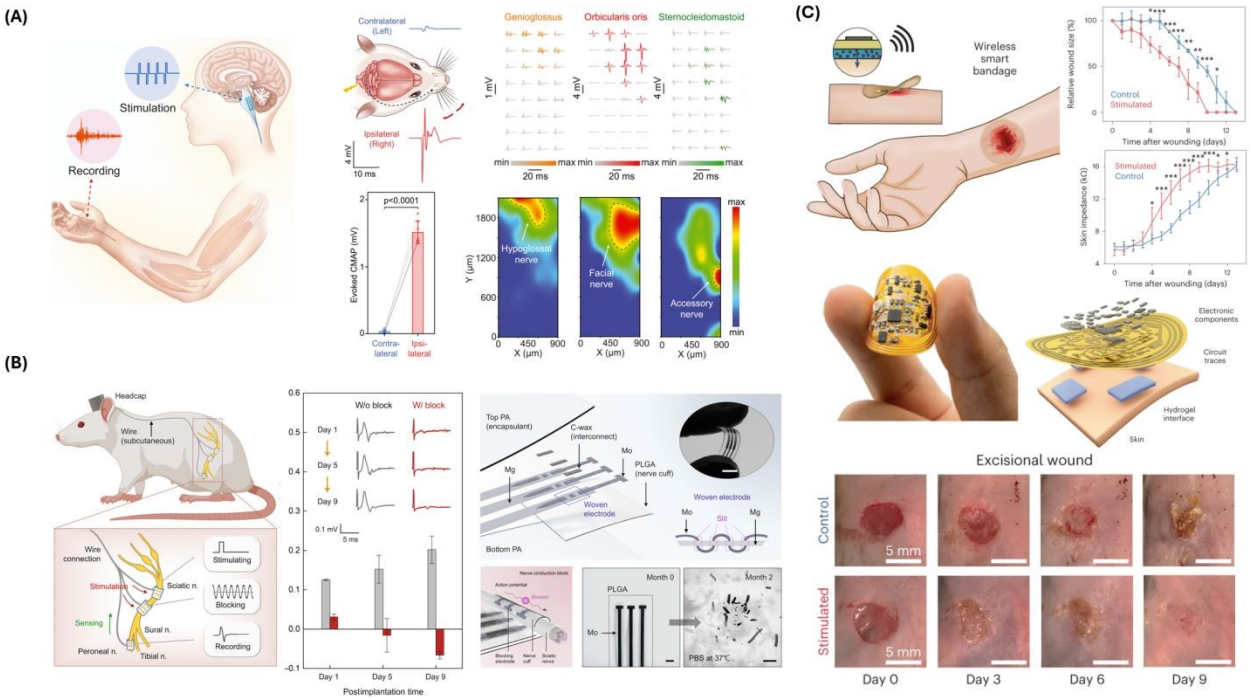

Figure 5. Electrical stimulation approaches and devices. (A) Intrinsically stretchable organic electronics for multimodal and conformal biointerfaces. Shows photograph of stretchable PEDOT:PSS interface on brain stem and octopus arm. Flexible, high-density array enables targeted neuromodulation for accurate regulation of specific muscle actions (right). Muscle responses in the tongue, whisker, and neck following electrical stimulation in the brainstem are recorded. Activation maps highlighting muscle activities illustrate the spatial arrangement of various nuclei within the brainstem. Reproduced from reference 137 with permission from *AAAS*, copyright 2022. **(B)** Schematic and structure of a bioresorbable peripheral nerve stimulator for electronic pain block. Data shows changes in action potential under stimulation for nerve conduction block for nine days. Reproduced from reference 141 with permission from *AAAS*, copyright 2022. **(C)** Schematic, design, and application of the wireless smart bandage for chronic wound care. In vivo evaluation shows the size and impedance of excisional wounds as a function of time, showing improved tissue healing with stimulation. Reproduced from reference 144 with permission from the copyright owner and *Springer Nature*, © 2022.

Table 3. Electrical Stimulation Devices

Stimulation Type	**Representative Designs**	**Aims/Characteristics**	**Application in Closed-Loop Systems**
Neural Stimulation	Wireless, bioresorbable stimulators, electrochemical corrosion, RF-powered devices	Precision targeting, wireless control, bioresorbability, reduced invasiveness	Chronic pain management, neuroregenerative therapy, functional restoration after spinal cord injury
Cardiac Stimulation	Capacitive coupling, flexible silicon transistors, biocompatible dielectric layers	Non-invasive, high-fidelity signal capture, extended operational lifetimes	Autonomous pacemakers, heart rhythm monitoring, real-time cardiac intervention
General Electrostimulation	Conformable electrodes, PEDOT	High flexibility, low impedance, long-term biocompatibility,	Continuous intraoperative monitoring, targeted

View Article Online
DOI: 10.1039/D4TB00782D

	coatings, capacitive sensors	superior signal-to-noise ratios	muscle stimulation, wearable health monitoring devices

4. Closed-Looped Wearable and Implantable Devices

Closed-looped wearable and implantable devices integrate biosensors and therapeutic components to provide continuous, real-time data on various physiological parameters. These systems harness advanced sensing strategies, including chemical, physical, and electrophysiological modalities, to detect a wide array of biomarkers with high specificity and sensitivity. Chemical sensors, employing redox-based, impedance-based, and transistor-based technologies, enable precise monitoring of metabolic and biochemical parameters. Physical sensors, utilizing thermal and pressure measurements, offer insights into the body's vital signs and mechanical properties. Electrophysiological sensors capture bioelectrical signals from physiological systems such as the skin, brain, and heart. Table 4 provides a summary of closed-loop system designs, showing the mechanisms, functions, and evaluations associated with each principal component.

An exemplary closed-loop system, designed by Mage et al., can control circulating drug concentrations within live animals.[146]. This system amalgamates an aptamer-based biosensor for real-time drug detection, a controller for dose calculation, and an infusion pump for drug delivery, integrated through a model of drug pharmacokinetics. This configuration addresses the variability in drug metabolism and response due to individual genetic and physiological differences, which traditional dosing methods based on body mass or surface area fail to consider. Mage et al. demonstrate the system's capability using doxorubicin, a chemotherapeutic agent with a narrow therapeutic index, highlighting its ability to maintain drug concentrations within a predetermined therapeutic range in rabbits and rats. The aptamer-based biosensor enables real-time quantification of drug concentrations directly from the bloodstream. It facilitates immediate feedback for the control algorithm, which dynamically adjusts the infusion pump's output to achieve the optimal drug concentration. In conclusion, this system is capable of real-time

View Article Online
DOI: 10.1039/D4TB00782D

adjustment to pharmacokinetic variations among individuals and acute pharmacokinetic perturbations induced by drug-drug interactions.

Yang et al. developed a wireless closed-loop theranostic contact lens for the monitoring and on-demand delivery of anti-glaucoma medication based on electrical sensing of intraocular pressure (IOP)[147]. This device uses a pressure sensor which utilizes a cantilever configuration to detect minute fluctuations in IOP (Fig. 6A). Anti-glaucoma drugs are encapsulated within a hydrogel layer and are released into the eye's aqueous chamber through iontophoresis, a process activated by detecting high-risk IOP conditions. The device's architecture integrates a pressure sensor, a wireless power transfer receiver, and drug storage within a hydrogel layer, all embedded in a soft contact lens. Experimental results reveal the device's wide linear monitoring range is suitable for capturing IOP fluctuations. Furthermore, the device demonstrated effective drug delivery through iontophoresis for enhanced drug permeation across the corneal barrier. These features position the wireless theranostic contact lens as a promising tool for proactively managing glaucoma, potentially transforming current therapeutic approaches by offering a more consistent and less invasive treatment option.

Closed-loop therapeutic devices have been widely utilized in developing prosthetic systems to assist amputees in regaining motor functions with sensory feedback. For instance, Osborn et al. designed a prosthesis with a multilayered electronic dermis (e-dermis)[148]. This e-dermis can neuromorphically perceive touch and pain, mimicking human skin's responsiveness to tactile stimuli. It incorporates resistive pressure sensor arrays for pressure mapping across the surface of the prosthetic hand. This enables the differentiation between innocuous (non-painful) and noxious (painful) touch, simulating the functions of mechanoreceptors and nociceptors in human skin. High local pressure detected by the e-dermis is processed to mimic the pain sensation. This processed sensation is fed back to the user in a closed-loop system through transcutaneous electrical nerve stimulation. The system provides tactile feedback that includes the perception of pain, similar to natural human sensory feedback. Wang et al. developed an electronic skin (e-skin) with a low-voltage operation that mimics the sensory feedback and mechanical softness of natural

View Article Online
DOI: 10.1039/D4TB00782D

skin (Fig. 6B)[149]. This e-skin integrates multimodal sensory perception, neuromorphic signal processing, and responsive actuation within a monolithically integrated architecture that eliminates the need for rigid electronic components. The system achieves operation at low voltages by employing a high-permittivity elastomer, enhancing safety and energy efficiency for potential on-body applications. The e-skin incorporates pressure and temperature sensors and neuromorphic circuits capable of generating pulse-train signals for closed-loop actuation, emulating the biological sensorimotor functions. Experimental demonstrations on a live rat model validated the system's biomimetic capabilities, showcasing its application potential for improving prosthetic interfaces and robotic sensing systems (Fig. 6B). These advancements address previous challenges in system-level integration and offer a new approach to developing electrical skin with advanced sensory feedback functions.

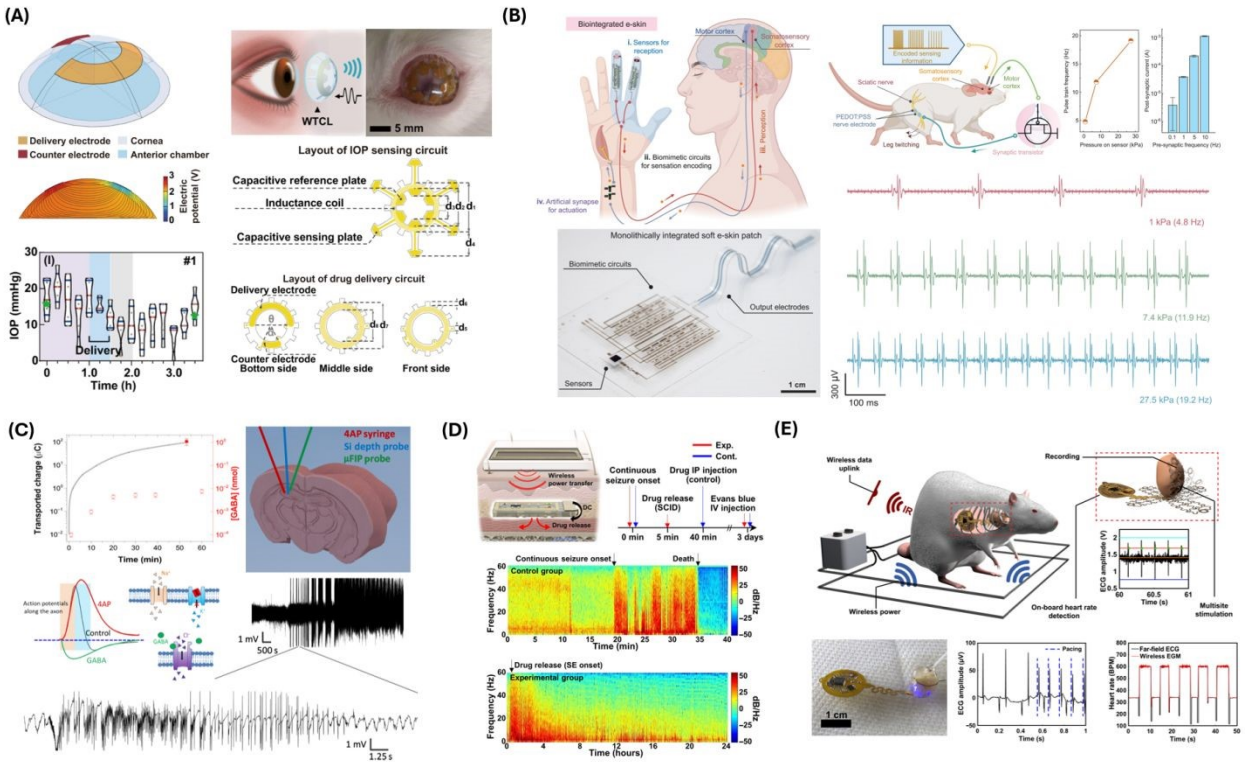

Figure 6. Integrated closed-loop therapeutic systems. (A) Schematic and design of the wireless theranostic contact lens for real-time, in situ intraocular pressure monitoring and drug delivery. In vivo sensing and therapeutic performance shown. Reproduced from reference 147 with permission from *Springer Nature* under terms of the Creative Commons CC BY license, copyright 2022. **(B)** Artificial soft e-skin system enables biomimetic signal transmission for sensation encoding and motor control. In vivo assessment in mouse model shows signals recorded from the motor cortex corresponding to pressures applied to the e-

View Article Online
DOI: 10.1039/D4TB00782D

skin system sensor. Reproduced from reference 149 with permission from *AAAS* copyright 2023. **(C)** Electrophoretic drug delivery for seizure control. Schematics show syringe placement for 4AP injection, Si depth probe, μFIP probe in the hippocampus. Following 4AP injection, intense SLEs are recorded. Reproduced from reference 150 with permission from *AAAS* copyright 2018. **(D)** Soft implantable drug delivery device integrated with wearables for seizure control. Shows in vivo results of seizure suppression with wireless control of subcutaneous medication delivery. Reproduced from reference 151 with permission from *AAAS* copyright 2021. **(E)** Wireless, implantable cardiac stimulation and recording for closed-loop pacing and defibrillation. Schematic illustrates a typical experiment setup and highlights device mechanics and operational capabilities. Reproduced from reference 153 with permission from *AAAS* copyright 2022.

Several closed-loop therapeutic devices have been developed for seizure control. For example, Proctor et al. engineered an electrophoretic drug delivery system that combines a microfluidic ion pump (μFIP) with a neural probe[150]. This system autonomously detects seizures by recording brain activity. It delivers γ-aminobutyric acid (GABA) directly to the brain when a seizure is detected (Fig. 6C). The μFIP operates by electrophoretically moving ions across an ion exchange membrane, allowing for precise, solvent-free drug delivery. This method avoids the risk of increased local pressure and potential edemas associated with traditional delivery systems. In tests with a rodent epilepsy model, the device demonstrated its ability to detect and interrupt seizure activity effectively, highlighting its potential for neural interfacing and treating neurological disorders.

Another representative closed-loop device was developed by Joo et al., which addresses neurological emergencies through a sophisticated sensing and treatment mechanism[151]. The system monitors EEG signals using a wearable electrophysiology sensor attached to the subject's head, continuously capturing characteristics such as frequency and amplitude to detect seizures. These sensors measure critical functions, including the onset and duration of seizures (Fig. 6D). When the system detects a seizure lasting more than 5 minutes, it diagnoses the condition as status epilepticus, necessitating immediate pharmaceutical intervention. Treatment involves a soft implantable drug delivery device (SID) that releases medication, typically benzodiazepines, upon receiving a command signal. The portable device processes the EEG data and, upon seizure detection, sends a wireless command to the wearable power transmitter. This transmitter generates a radio frequency signal, which the SID converts into a DC voltage, inducing electrolysis and triggering drug release. The control of this system is managed by a portable

View Article Online
DOI: 10.1039/D4TB00782D

device, which runs a seizure detection algorithm that processes the EEG data in real-time. Upon detecting status epilepticus, it sends a command to the wearable power transmitter, initiating the drug release process by the SID. This closed-loop control ensures timely and effective treatment during seizure events. The logical flow diagram of the closed-loop system includes EEG monitoring by the wearable sensor, data processing, seizure detection by the portable device, and drug release. This integration of wireless communication and power transmission ensures real-time monitoring and rapid intervention, maintaining the mechanical softness and miniaturization of the SID for minimally invasive subcutaneous implantation.

Recent advancements have introduced fully implantable, wireless, and battery-less systems that support artificial intelligence (AI) algorithms for autonomous closed-loop neurorecording and neuromodulation. A notable example is the implantable device developed by Ouyang et al., which offers high-performance recording of EEGs, EMGs, and body temperature[152]. This device also supports closed-loop neuromodulation via optogenetics and pharmacology and operates without physical tethers or batteries, thereby allowing for studies with freely behaving small animals. The device incorporates a system-on-a-chip with Bluetooth Low Energy for data transmission and an embedded deep-learning module for autonomous operation, providing neurorecording capabilities comparable to gold-standard wired systems. Specifically, the system monitors the characteristics of neural pulse patterns, including amplitude and frequency, and measures critical functions such as neural activity and physiological responses. Upon detecting abnormal neural signals associated with epileptic seizures, the system initiates appropriate treatment protocols, such as optogenetic stimulation or drug delivery, through a control module that seamlessly integrates monitoring and therapeutic actions. The logical flow of this closed-loop system encompasses real-time data acquisition, analysis via AI algorithms, and immediate therapeutic intervention, thereby enhancing the efficacy of neuromodulation in research and potential clinical applications.

An article by Ausra et al. presents a closed-loop device integrating electrical and optoelectronic sensing mechanisms into a flexible, conformal array for real-time cardiac monitoring and control (Fig. 6E) [153]. The device features platinum electrodes that capture electrical signals, such as ECGs, and an analog

View Article Online
DOI: 10.1039/D4TB00782D

front-end circuit (AD8233) amplifies and filters these signals before conversion to digital format by a microcontroller (μC). The μC performs onboard heart rate detection using an automatic thresholding method, enabling real-time data processing and transmission. Optoelectronic components, including micro-LEDs (μ-ILEDs), provide precise, targeted stimulation with mechanisms to measure light propagation and thermal effects, ensuring safe and effective operation. The device is wirelessly powered via magnetic resonant coupling. It communicates using infrared (IR) signals, allowing for untethered, continuous operation (Fig. 6E). The flexible, ultrathin array ensures intimate contact with the heart, enhancing signal accuracy and reliability. This device monitors heart rate, ECG, and optical and thermal responses, measuring essential functions for diagnosing and treating cardiovascular pathologies. When irregularities like arrhythmias are detected, appropriate therapies, including pacing and defibrillation, are delivered through an integrated control module that facilitates continuous monitoring and real-time therapeutic intervention. The logical flow of the closed-loop system involves signal acquisition, data processing for heart rate detection, decision-making for therapeutic intervention, and execution of stimulation protocols, ensuring seamless cardiac function management. This system's potential for advanced cardiovascular research and therapy is demonstrated in freely moving animal models, highlighting its application for long-term studies and real-time treatment of heart conditions.

Roger's group introduces a novel miniaturized bio-optoelectronic implant that employs optical stimulation through microscale light-emitting diodes to activate opsins[154]. This implant includes a soft, high-precision biophysical sensor system for continuous organ function monitoring. Control module and data analytics enabled real-time closed-loop operation, effectively detecting and correcting pathological behaviors. In rat models, this system successfully normalized bladder function through automated, closed-loop optogenetic neuromodulation of bladder sensory afferents. This all-optical method offers chronic stability and specific cell-type stimulation potential. The study underscores the adaptability of this approach beyond bladder-related conditions. By modifying the stimulation and sensing module and incorporating various sensors and actuators, this technology can address a broad range of PNS-related physiological and

View Article Online
DOI: 10.1039/D4TB00782D

pathophysiological scenarios. The integrated control module and data analytics allow for real-time adjustments, paving the way for future closed-loop technologies in PNS disease treatment and offering targeted and effective alternatives to non-specific pharmacological or electrical stimulation methods.

Table 4. Closed-Loop System Design

Component	Function	Key Technologies	Advantages	Challenges
Biosensors	Detect physiological signals and biomarkers	Chemical sensors (redox, impedance, transistor-based), physical sensors (pressure, temperature), electrophysiological sensors	Real-time monitoring, high sensitivity, specificity, integration with therapeutic devices	Biocompatibility, long-term stability, avoiding signal interference
Control Modules	Process sensor data, make decisions, and control therapeutic devices	Microcontrollers, wireless communication, AI algorithms	Autonomous operation, personalized therapy adjustments, real-time feedback	Power consumption, data security, algorithm accuracy
Drug Delivery Systems	Administer drugs based on real-time physiological data	Microneedles, implantable devices, ingestible capsules	Precise dosing, targeted delivery, reduced side effects	Integration with sensors, ensuring timely and appropriate drug release
Electrical Stimulation Devices	Provide electrical stimulation to target tissues based on sensor feedback	Neural stimulators, cardiac stimulators, general electrostimulation devices	Targeted therapy, non-invasive options, real-time adjustments	Electrical safety, ensuring effective stimulation without causing damage
Data Management Systems	Collect, store, and analyze data from biosensors and control modules	Cloud storage, data encryption, machine learning analytics	Long-term data tracking, secure storage, enhanced decision-making	Privacy concerns, managing large datasets, maintaining data integrity
Power Supply	Provide energy to all components of the closed-loop system	Batteries, wireless power transfer, energy harvesting	Sustained operation, minimizing need for recharging or battery replacement	Power efficiency, ensuring continuous power supply, managing heat generation

View Article Online
DOI: 10.1039/D4TB00782D

5. Challenges and Future Prospects

Wearable and implantable sensors are essential for personalized medicine and closed-loop therapeutic systems. Nevertheless, the development and deployment of these sensors face numerous challenges that must be addressed to ensure their efficacy, safety, and widespread adoption. These challenges span biocompatibility, signal interference, power supply, miniaturization, and long-term durability. Addressing these multifaceted challenges is essential for advancing biosensing technologies and realizing their full potential in improving patient outcomes and healthcare delivery. This section delves into the specific obstacles encountered in wearable and implantable sensor technologies to discuss each aspect and highlight the ongoing research and innovations to overcome these barriers (Table 5).

5.1 Biocompatibility

Wearable and implantable sensors must be constructed from materials that do not elicit adverse reactions when in contact with biological tissues. The long-term implantation of these sensors can lead to fibrosis, where fibrous tissue forms around the sensor, insulating it from its target tissues and impairing its functionality[155]. Innovations in materials science are crucial to developing biocompatible sensors that can operate effectively over extended periods without causing harm or being rejected by the body[156]. In vivo, chemical sensors must navigate a dynamic environment where protein adsorption and subsequent cell adhesion can significantly alter their performance. The initial response to implantation involves a rapid accumulation of proteins on the sensor surface, leading to various biological reactions that can compromise the sensor's function. For instance, this process often results in thrombus formation in blood, while in subcutaneous and neural tissues, it leads to inflammatory reactions and fibrous encapsulation [155]. Ongoing research to improve the biocompatibility of wearable and implantable biosensors includes several innovative approaches. Researchers are developing sensors made from biodegradable materials such as polylactic acid (PLA) and polyglycolic acid (PGA), which gradually dissolve in the body, reducing the risk of chronic inflammation and eliminating the need for surgical removal [157]. Hydrogel-based sensors, which mimic the properties of natural tissue, and conductive polymers like polyaniline and PEDOT are used to create flexible, soft sensors that maintain functionality while ensuring compatibility with the body [158, 159].

View Article Online
DOI: 10.1039/D4TB00782D

Surface coatings such as PEGylation or zwitterionic coatings can prevent protein adsorption and reduce immune responses [160]. Incorporating nanomaterials like graphene and gold nanoparticles can enhance sensor functionality while maintaining biocompatibility [161]. Bioinspired designs that mimic natural structures, smart drug delivery systems that manage biocompatibility issues in real-time, and 3D printing to create personalized sensors all contribute to improved integration with tissues. Additionally, research into self-healing materials and the integration of microfluidic systems for localized cooling or therapeutic delivery further enhance the biocompatibility and longevity of these sensors [162]. These efforts aim to create effective, reliable biosensors that seamlessly integrate with the human body, minimizing adverse reactions and enhancing the overall user experience.

5.2 Signal Interference

Wearable and implantable sensors are prone to various types of signal interference, which can significantly affect the accuracy of the data they collect. For wearable sensors, motion artifacts caused by body movements can distort readings, making it difficult to obtain precise measurements [163, 164]. Motion artifacts are especially challenging in wearable EEG and photoplethysmography (PPG) devices, as these artifacts are typically at least ten times greater in amplitude than bio-signals. The smaller amplitude and non-stationary waveform of EEG signals and the sensor displacement in PPG monitoring exacerbate the impact of motion artifacts on EEG and PPG sensors. Various hardware and software techniques have been developed to address these issues to remove or compensate for motion artifacts. These include using different electrode types, analog readout circuits, and advanced signal processing techniques [164]. On the other hand, implantable sensors can be affected by electromagnetic interference (EMI) from other electronic devices, which can corrupt the signals [165]. To mitigate these risks, device engineers employ various shielding and filtering techniques to block or reduce the impact of EMI. This includes using capacitors for passive filtering and the design of feedthrough filters that can separate noise from the intended signal [166, 167]. However, ensuring complete protection is challenging, as these devices must still interact with the body and external devices for monitoring and treatment purposes. Developing robust algorithms and hardware

View Article Online
DOI: 10.1039/D4TB00782D

that can filter out noise and provide accurate and reliable data is essential to overcoming these challenges [168].

5.3 Power Supply

One of the most crucial challenges for wearable and implantable sensors is ensuring a reliable and sustainable power source. Wearable sensors often rely on batteries, which require frequent recharging or replacement, limiting their practicality for continuous monitoring. Implantable sensors face even more significant challenges, as battery replacement is impractical or impossible without invasive procedures. To address this, researchers are exploring energy harvesting technologies that can convert physiological activities, such as body movements and heat, into electrical power [169]. Thermoelectric generators (TEGs) utilize the temperature gradient between the human body and the environment to generate power [170]. These generators convert body heat into electrical energy, enabling the continuous operation of medical devices without needing battery replacement. Another promising approach is the use of piezoelectric materials, which generate electricity in response to mechanical stress [171]. These materials can harvest energy from body movements, such as walking or heartbeats, to power implantable sensors. Additionally, triboelectric nanogenerators (TENGs) leverage the contact electrification effect to produce energy from movements like muscle contractions and even from the flow of body fluids [172]. Integrating these energy harvesting mechanisms makes it feasible to develop self-sustaining, battery-free wearable and implantable biosensors, significantly enhancing their practicality and reliability for long-term health monitoring. These innovations aim to provide a continuous power supply, extending the operational life of these sensors without the need for external interventions.

5.4 Miniaturization and Integration

The trend toward miniaturization in sensor technology aims to make devices less intrusive and more comfortable for continuous wear or implantation. However, achieving small form factors while maintaining or enhancing functionality poses significant technical challenges. Miniaturizing sensors can limit battery life and functional capabilities, necessitating careful design to balance size and performance. Integrating multiple sensing capabilities into a single, compact device without compromising accuracy or

View Article Online
DOI: 10.1039/D4TB00782D

reliability is an ongoing area of research, requiring advances in materials science and engineering [173]. The development of nano- and microdevices for biotechnology and wearables focuses on high point-of-care bioanalysis and various applications in life sciences. This involves the control of nanoscale to functional microarchitectures in different materials. Several vital areas include nanophotonics, advanced nanomaterials, light generation, microfluidics, nanofluidics, signal waveguiding, and quantum circuits[173-177].

5.5 Durability and Longevity

Wearable and implantable sensors must withstand the physical and chemical challenges the human body poses. These include mechanical stress from movements, corrosion from bodily fluids, and potential biological fouling. Ensuring that sensors are robust enough to endure these conditions without degrading performance over time is crucial for their reliability and usability. This requires the development of materials and coatings that can provide long-term protection while maintaining sensor functionality. Flexible and stretchable materials such as silicone elastomers, polyurethane, and thermoplastic elastomers are being utilized to cope with mechanical stress from bodily movements, which allow sensors to bend, stretch, and conform to the body's contours [178, 179]. PEDOT is used for their excellent electrical conductivity and flexibility [158]. Nanomaterials such as gold, silver, and platinum nanoparticles or nanowires are incorporated into sensors to enhance their electrical properties [180]. To protect against corrosion from bodily fluids, sensors are often coated with biostable and corrosion-resistant materials. Parylene, a commonly used coating, provides a thin, conformal barrier that protects the sensor components from moisture and chemical degradation [181]. Other coatings, such as titanium nitride (TiN) and diamond-like carbon (DLC), offer robust protection against corrosion while maintaining electrical conductivity [182, 183]. Additionally, Anti-fouling coatings such as PEG and zwitterionic polymers are being developed to prevent biofouling to prolong device functional stability[160].

Table 5. Challenges and Recent Developments

Challenge	Description	Recent Developments
Biocompatibility	Ensuring sensors do not elicit adverse reactions or cause harm over long-term implantation.	Biodegradable materials, hydrogel-based sensors, conductive polymers, surface

View Article Online
DOI: 10.1039/D4TB00782D

		coatings, nanomaterials, bioinspired designs, and 3D printing for personalization.
Signal Interference	Addressing motion artifacts and EMI that distort sensor readings.	Advanced signal processing, different electrode types, analog readout circuits, shielding and filtering techniques.
Power Supply	Providing a reliable and sustainable power source for continuous operation of sensors.	Energy harvesting technologies, flexible and high-efficiency batteries.
Miniaturization	Achieving small form factors while maintaining functionality and ensuring comfort for continuous wear or implantation.	Nanotechnology, nano- and microdevices, high point-of-care bioanalysis, compact device integration.
Durability and Longevity	Ensuring sensors withstand mechanical stress, corrosion from bodily fluids, and biological fouling without performance degradation over time.	Flexible and stretchable materials, conductive materials, anti-fouling coatings, durable surface coatings.

6. Conclusion and outlook

The future of wearable and implantable biosensors is a subject of significant interest in the medical and technological communities, given their potential to revolutionize how healthcare is delivered and personalized. Chemical sensors, such as redox-based, impedance-based, and transistor-based sensors, allow for precisely detecting biomarkers and metabolic parameters. Physical sensors, including pressure and temperature sensors, provide critical data on vital signs and physiological conditions. Electrophysiological sensors capture bioelectrical activities, offering insights into neural and muscular functions. The integration of these sensing strategies into wearable and implantable devices has paved the way for the development of sophisticated closed-loop therapeutic systems. These devices offer continuous monitoring of physiological parameters to provide valuable data that can lead to earlier disease detection, tailored treatment regimens, and potentially better patient outcomes. This concluding outlook addresses the trajectory, potential innovations, and challenges that may shape the evolution of these technologies.

Advances in nanotechnology, flexible electronics, and biocompatible materials are expected to drive the development of more sensitive, specific, and user-friendly biosensors. Nanoscale sensors could

View Article Online
DOI: 10.1039/D4TB00782D

detect low-abundance biomarkers to enhance disease diagnosis and monitoring. Flexible and stretchable electronic components could improve the comfort and wearability of these devices, increasing user adoption. Furthermore, the use of biocompatible and bioresorbable materials in implantable biosensors could reduce long-term implantation risks, such as infection or device rejection. The integration of biosensors with digital health platforms and electronic health records is anticipated to enhance the management and monitoring of patient health. Real-time data transmission to healthcare providers can facilitate remote monitoring and early intervention, improving the responsiveness and effectiveness of medical care. Applying AI and machine learning to these data streams can further enable predictive modeling of disease progression and treatment outcomes.

Despite the potential benefits, the widespread adoption of wearable and implantable biosensors faces several additional challenges. Regulatory approval processes, data privacy and security concerns, and the need for standardization in data interpretation present significant hurdles. Moreover, ensuring the accessibility and affordability of these technologies is critical to their broader application in healthcare, particularly across diverse socioeconomic groups.

The outlook for wearable and implantable biosensors in healthcare is broadly positive, with substantial advancements on the horizon that promise to personalize further and improve patient care. However, realizing this potential will require overcoming technical, regulatory, and ethical challenges. Continuous technology innovation, alongside efforts to address these challenges, will be key to integrating these devices into mainstream healthcare and unlocking their full potential in patient health service.

View Article Online
DOI: 10.1039/D4TB00782D

Author Contributions
Z.Z., R.Z., I.P., and Z.X. wrote the manuscript. Y.J. supervised the work and edited the manuscript.

Declaration of Interests
The authors declare no conflict of interest.

Acknowledgments
This work was supported by the start-up funding from the University of Pennsylvania.

View Article Online
DOI: 10.1039/D4TB00782D

References

1. E. B. Bahadir and M. K. Sezgintürk, *Artif Cell Nanomed B*, 2016, **44**, 248-262.
2. D. Sadighbayan, M. Hasanzadeh and E. Ghafar-Zadeh, *Trac-Trend Anal Chem*, 2020, **133**.
3. J. R. Sempionatto, J. A. Lasalde-Ramírez, K. Mahato, J. Wang and W. Gao, *Nat Rev Chem*, 2022, **6**, 899-915.
4. R. Frank and R. Hargreaves, *Nat Rev Drug Discov*, 2003, **2**, 566-580.
5. H. Sohrabi, N. Bolandi, A. Hemmati, S. Eyvazi, S. Ghasemzadeh, B. Baradaran, F. Oroojalian, M. R. Majidi, M. de la Guardia and A. Mokhtarzadeh, *Microchem J*, 2022, **177**.
6. P. P. Joshi, S. A. Merchant, Y. D. Wang and D. W. Schmidtke, *Anal Chem*, 2005, **77**, 3183-3188.
7. J. J. Liu, Y. F. Xu, S. K. Liu, S. X. Yu, Z. R. Yu and S. S. Low, *Biosensors-Basel*, 2022, **12**.
8. F. Schachinger, H. C. Chang, S. Scheiblbrandner and R. Ludwig, *Molecules*, 2021, **26**.
9. M. A. Arugula and A. Simonian, *Meas Sci Technol*, 2014, **25**.
10. A. K. H. Cheng, D. Sen and H. Z. Yu, *Bioelectrochemistry*, 2009, **77**, 1-12.
11. N. Kalita, S. Gogoi, S. D. Minteer and P. Goswami, *Acs Meas Sci Au*, 2023, **3**, 404-433.
12. P. Bollella and L. Gorton, *Curr Opin Electroche*, 2018, **10**, 157-173.
13. Y. F. Fan, Z. B. Guo and G. B. Ge, *Biosensors-Basel*, 2023, **13**.
14. A. Yarman, C. Schulz, C. Sygmund, R. Ludwig, L. Gorton, U. Wollenberger and F. W. Scheller, *Electroanal*, 2014, **26**, 2043-2048.
15. W. J. Zhang and G. X. Li, *Anal Sci*, 2004, **20**, 603-609.
16. X. F. Jin, A. Cai, T. L. Xu and X. J. Zhang, *Interd Mater*, 2023, **2**, 290-307.
17. K. Scholten and E. Meng, *Int J Pharmaceut*, 2018, **544**, 319-334.
18. L. Sakalauskiene, A. Popov, A. Kausaite-Minkstimiene, A. Ramanavicius and A. Ramanaviciene, *Biosensors*, 2022, **12**, 320.
19. A. B. Karol, G. O'Malley, R. Fallurin and C. J. Levy, *Endocr Pract*, 2023, **29**, 214-220.
20. Y. Q. Liu, Q. Yu, L. Ye, L. Yang and Y. Cui, *Lab Chip*, 2023, **23**, 421-436.
21. I. S. Kucherenko, Y. V. Topolnikova and O. O. Soldatkin, *Trac-Trend Anal Chem*, 2019, **110**, 160-172.
22. R. Sainz, M. del Pozo, L. Vázquez, M. Vilas-Varela, J. Castro-Esteban, E. Blanco, M. D. Petit-Domínguez, C. Quintana and E. Casero, *Anal Chim Acta*, 2022, **1208**.
23. W. Gao, S. Emaminejad, H. Y. Y. Nyein, S. Challa, K. Chen, A. Peck, H. M. Fahad, H. Ota, H. Shiraki, D. Kiriya, D.-H. Lien, G. A. Brooks, R. W. Davis and A. Javey, *Nature*, 2016, **529**, 509-514.
24. X. T. Zheng, Z. Yang, L. Sutarlie, M. Thangaveloo, Y. Yu, N. A. B. M. Salleh, J. S. Chin, Z. Xiong, D. L. Becker, X. J. Loh, B. C. K. Tee and X. Su, *Sci Adv*, **9**, eadg6670.
25. A. K. H. Cheng, B. Ge and H. Z. Yu, *Anal Chem*, 2007, **79**, 5158-5164.
26. S. Y. Lam, H. L. Lau and C. K. Kwok, *Biosensors-Basel*, 2022, **12**.
27. S. Y. Tan, C. Acquah, A. Sidhu, C. M. Ongkudon, L. S. Yon and M. K. Danquah, *Crit Rev Anal Chem*, 2016, **46**, 521-537.
28. N. Nakatsuka, K.-A. Yang, J. M. Abendroth, K. M. Cheung, X. Xu, H. Yang, C. Zhao, B. Zhu, Y. S. Rim, Y. Yang, P. S. Weiss, M. N. Stojanović and A. M. Andrews, *Science*, 2018, **362**, 319-324.
29. T. Hianik and J. Wang, *Electroanal*, 2009, **21**, 1223-1235.
30. L. Hosseinzadeh and M. Mazloum-Ardakani, *Adv Clin Chem*, 2020, **99**, 237-279.
31. X. Y. Kou, X. J. Zhang, X. J. Shao, C. Y. Jiang and L. M. Ning, *Anal Bioanal Chem*, 2020, **412**, 6691-6705.
32. A. M. Onas, C. Dascalu, M. D. Raicopol and L. Pilan, *Biosensors-Basel*, 2022, **12**.
33. C. Wang and Q. Zhao, *Biosens Bioelectron*, 2020, **167**.
34. L. Zhou, J. P. Wang, D. J. Li and Y. B. Li, *Food Chem*, 2014, **162**, 34-40.
35. J. Zhang, Y. Q. Chai, R. Yuan, Y. L. Yuan, L. J. Bai, S. B. Xie and L. P. Jiang, *Analyst*, 2013, **138**, 4558-4564.
36. P. J. Conroy, S. Hearty, P. Leonard and R. J. O'Kennedy, *Semin Cell Dev Biol*, 2009, **20**, 10-26.

View Article Online
DOI: 10.1039/D4TB00782D

37. S. Sharma, H. Byrne and R. J. O'Kennedy, *Essays Biochem*, 2016, **60**, 9-18.
38. A. K. Trilling, J. Beekwilder and H. Zuilhof, *Analyst*, 2013, **138**, 1619-1627.
39. X. Q. Zeng, Z. H. Shen and R. Mernaugh, *Anal Bioanal Chem*, 2012, **402**, 3027-3038.
40. A. Makaraviciute and A. Ramanaviciene, *Biosens Bioelectron*, 2013, **50**, 460-471.
41. A. Campu, I. Muresan, A. M. Craciun, S. Cainap, S. Astilean and M. Focsan, *Int J Mol Sci*, 2022, **23**.
42. D. Çimen, N. Bereli, S. Günaydin and A. Denizli, *Talanta*, 2020, **219**.
43. X. J. Liao, H. J. Xiao, J. T. Cao, S. W. Ren and Y. M. Liu, *Talanta*, 2021, **233**.
44. A. Pourali, M. R. Rashidi, J. Barar, G. Pavon-Djavid and Y. Omidi, *Trac-Trend Anal Chem*, 2021, **134**.
45. M. D. Gholami, A. P. O'Mullane, P. Sonar, G. A. Ayoko and E. L. Izake, *Anal Chim Acta*, 2021, **1185**, 339082.
46. A. D. Luong, I. Roy, B. D. Malhotra and J. H. T. Luong, *Sensor Actuator Rep*, 2021, **3**.
47. C. Sabu, T. K. Henna, V. R. Raphey, K. P. Nivitha and K. Pramod, *Biosens Bioelectron*, 2019, **141**.
48. I. A. P. Thompson, J. Saunders, L. Zheng, A. A. Hariri, N. Maganzini, A. P. Cartwright, J. Pan, S. Yee, C. Dory, M. Eisenstein, J. Vuckovic and H. T. Soh, *Sci Adv*, **9**, eadh4978.
49. J. S. Daniels and N. Pourmand, *Electroanal*, 2007, **19**, 1239-1257.
50. F. Lisdat and D. Schäfer, *Anal Bioanal Chem*, 2008, **391**, 1555-1567.
51. H. S. Magar, R. Y. A. Hassan and A. Mulchandani, *Sensors-Basel*, 2021, **21**.
52. R. A. D. de Faria, L. G. D. Heneine, T. Matencio and Y. Messaddeq, *International Journal of Biosensors & Bioelectronics*, 2019.
53. M. E. Strong, J. R. Richards, M. Torres, C. M. Beck and J. T. La Belle, *Biosens Bioelectron*, 2021, **177**.
54. A. K. Assaifan, F. A. Alqahtani, S. Alnamlah, R. Almutairi and H. I. Alkhammash, *BioChip Journal*, 2022, **16**, 197-206.
55. H. T. N. Le, D. Kim, L. M. T. Phan and S. Cho, *Talanta*, 2022, **237**, 122907.
56. E. Katz and I. Willner, *Electroanal*, 2003, **15**, 913-947.
57. R. D. Munje, S. Muthukumar and S. Prasad, *Sensor Actuat B-Chem*, 2017, **238**, 482-490.
58. T. Yang, S. Wang, H. L. Jin, W. W. Bao, S. M. Huang and J. C. Wang, *Sensor Actuat B-Chem*, 2013, **178**, 310-315.
59. Y. C. Syu, W. E. Hsu and C. T. Lin, *Ecs J Solid State Sc*, 2018, **7**, Q3196-Q3207.
60. T. Wadhera, D. Kakkar, G. Wadhwa and B. Raj, *J Electron Mater*, 2019, **48**, 7635-7646.
61. S. K. Krishnan, N. Nataraj, M. Meyyappan and U. Pal, *Anal Chem*, 2023, DOI: 10.1021/acs.analchem.2c03399.
62. A. B. Kharitonov, M. Zayats, A. Lichtenstein, E. Katz and I. Willner, *Sensor Actuat B-Chem*, 2000, **70**, 222-231.
63. C. S. Lee, S. K. Kim and M. Kim, *Sensors-Basel*, 2009, **9**, 7111-7131.
64. G. J. Zhang and Y. Ning, *Anal Chim Acta*, 2012, **749**, 1-15.
65. S. Yuvaraja, A. Nawaz, Q. Liu, D. Dubal, S. G. Surya, K. N. Salama and P. Sonar, *Chem Soc Rev*, 2020, **49**, 3423-3460.
66. S. Mao, in *Graphene Bioelectronics*, Elsevier, 2018, pp. 113-132.
67. H. U. Khan, M. E. Roberts, O. Johnson, W. Knoll and Z. A. Bao, *Org Electron*, 2012, **13**, 519-524.
68. H. Tang, F. Yan, P. Lin, J. B. Xu and H. L. W. Chan, *Adv Funct Mater*, 2011, **21**, 2264-2272.
69. N. Nakatsuka, K. A. Yang, J. M. Abendroth, K. M. Cheung, X. B. Xu, H. Y. Yang, C. Z. Zhao, B. W. Zhu, Y. S. Rim, Y. Yang, P. S. Weiss, M. N. Stojanovic and A. M. Andrews, *Science*, 2018, **362**, 319-+.
70. M. I. Khan, K. Mukherjee, R. Shoukat and H. Dong, *Microsyst Technol*, 2017, **23**, 4391-4404.
71. M. T. Ghoneim, A. Nguyen, N. Dereje, J. Huang, G. C. Moore, P. J. Murzynowski and C. Dagdeviren, *Chem Rev*, 2019, **119**, 5248-5297.
72. J. Liu, N. Liu, Y. Xu, M. Wu, H. Zhang, Y. Wang, Y. Yan, A. Hill, R. Song, Z. Xu, M. Park, Y. Wu, J. L. Ciatti, J. Gu, H. Luan, Y. Zhang, T. Yang, H.-Y. Ahn, S. Li, W. Z. Ray, C. K. Franz, M.

View Article Online
DOI: 10.1039/D4TB00782D

R. MacEwan, Y. Huang, C. W. Hammill, H. Wang and J. A. Rogers, *Science*, 2024, **383**, 1096-1103.
73. M. Corsi, A. Paghi, S. Mariani, G. Golinelli, A. Debrassi, G. Egri, G. Leo, E. Vandini, A. Vilella, L. Dähne, D. Giuliani and G. Barillaro, *Adv Sci*, 2022, **9**.
74. Z. Y. Nie, J. W. Kwak, M. D. Han and J. A. Rogers, *Adv Mater*, 2023, DOI: 10.1002/adma.202205609.
75. U. P. Claver and G. Zhao, *Adv Eng Mater*, 2021, **23**.
76. R. Yang, A. Dutta, B. Li, N. Tiwari, W. Zhang, Z. Niu, Y. Gao, D. Erdely, X. Xin, T. Li and H. Cheng, *Nature Communications*, 2023, **14**, 2907.
77. Q. P. Lin, J. Huang, J. L. Yang, Y. Huang, Y. F. Zhang, Y. J. Wang, J. M. Zhang, Y. Wang, L. L. Yuan, M. K. Cai, X. Y. Hou, W. X. Zhang, Y. L. Zhou, S. G. Chen and C. F. Guo, *Adv Healthc Mater*, 2020, **9**.
78. S. Lee, S. Franklin, F. A. Hassani, T. Yokota, M. O. G. Nayeem, Y. Wang, R. Leib, G. Cheng, D. W. Franklin and T. Someya, *Science*, 2020, **370**, 966-970.
79. Q. Su, Q. Zou, Y. Li, Y. Z. Chen, S. Y. Teng, J. T. Kelleher, R. Nith, P. Cheng, N. Li, W. Liu, S. L. Dai, Y. D. Liu, A. Mazursky, J. Xu, L. H. Jin, P. Lopes and S. H. Wang, *Sci Adv*, 2021, **7**.
80. J. W. Yin, S. N. Guo, M. F. E, H. Liu, Z. H. Liu, W. Y. Ding, D. M. Li and Y. X. Cui, *Adv Eng Mater*, 2023, **25**.
81. S. W. Min, D. H. Kim, D. J. Joe, B. W. Kim, Y. H. Jung, J. H. Lee, B. Y. Lee, I. Doh, J. H. An, Y. N. Youn, B. Joung, C. D. Yoo, H. S. Ahn and K. J. Lee, *Adv Mater*, 2023, **35**.
82. H. Y. Wang, W. Q. Wang, J. J. Kim, C. Y. Wang, Y. Wang, B. H. Wang, S. Lee, T. Yokota and T. Someya, *Sci Adv*, 2023, **9**.
83. J. A. Barreiros, A. Xu, S. Pugach, N. Iyengar, G. Troxell, A. Cornwell, S. Hong, B. Selman and R. F. Shepherd, *Sci Robot*, 2022, **7**.
84. Y. F. Lu, H. J. Zhang, Y. Zhao, H. D. Liu, Z. T. Nie, F. Xu, J. X. Zhu and W. Huang, *Adv Mater*, 2024, DOI: 10.1002/adma.202310613.
85. L. Dan and A. L. Elias, *Adv Healthc Mater*, 2020, **9**.
86. W. Fan, T. Liu, F. Wu, S. J. Wang, S. B. Ge, Y. H. Li, J. L. Liu, H. R. Ye, R. X. Lei, C. Wang, Q. L. Che and Y. Li, *Acs Nano*, 2023, **17**, 21073-21082.
87. H. Yu, Z. Hu, J. He, Y. Ran, Y. Zhao, Z. Yu and K. Tai, *Nature Communications*, 2024, **15**, 2521.
88. R. Y. Liu, Z. L. Wang, K. Fukuda and T. Someya, *Nat Rev Mater*, 2022, **7**, 870-886.
89. C. Shi, V. Andino-Pavlovsky, S. A. Lee, T. Costa, J. Elloian, E. E. Konofagou and K. L. Shepard, *Sci Adv*, 2021, **7**.
90. C. Y. Wang, Y. X. Zhang, F. Han and Z. D. Jiang, *Micromachines-Basel*, 2023, **14**.
91. S. Xie, *Electronics-Switz*, 2022, **11**.
92. G. Zamora-Mejia, J. Martinez-Castillo, A. Diaz-Sanchez, J. M. Rocha-Perez, A. L. Herrera-May, U. G. Zapata-Rodriguez and V. H. Carbajal-Gomez, *Electronics-Switz*, 2022, **11**.
93. S. R. Madhvapathy, M. I. Bury, L. W. Wang, J. L. Ciatti, R. Avila, Y. Huang, A. K. Sharma and J. A. Rogers, *Nature Biomedical Engineering*, 2024, DOI: 10.1038/s41551-024-01183-w.
94. H. Ullah, M. A. Wahab, G. Will, M. R. Karim, T. Pan, M. Gao, D. Lai, Y. Lin and M. H. Miraz, *Journal*, 2022, **12**.
95. X. Yang, T. Zhou, T. J. Zwang, G. Hong, Y. Zhao, R. D. Viveros, T.-M. Fu, T. Gao and C. M. Lieber, *Nat Mater*, 2019, **18**, 510-517.
96. B. J. Woodington, J. Lei, A. Carnicer-Lombarte, A. Güemes-González, T. E. Naegele, S. Hilton, S. El-Hadwe, R. A. Trivedi, G. G. Malliaras and D. G. Barone, *Sci Adv*, **10**, eadl1230.
97. H. Ullah, M. A. Wahab, G. Will, M. R. Karim, T. S. Pan, M. Gao, D. K. Lai, Y. Lin and M. H. Miraz, *Biosensors-Basel*, 2022, **12**.
98. B. Lv, X. T. Chen and C. G. Liu, *Sensors-Basel*, 2020, **20**.
99. Y. Mouhamad, T. Mortensen, A. Holder, A. R. Lewis, T. G. G. Maffeis and D. Deganello, *Rsc Adv*, 2016, **6**, 105206-105210.
100. Y. L. Wu, Y. L. Ma, H. Y. Zheng and S. Ramakrishna, *Mater Design*, 2021, **211**.

View Article Online
DOI: 10.1039/D4TB00782D

101. S. L. Dai, X. Liu, Y. D. Liu, Y. T. Xu, J. Y. Zhang, Y. Wu, P. Cheng, L. Z. Xiong and J. Huang, *Adv Mater*, 2023, **35**.
102. Y. He, Y. Cheng, C. Yang and C. F. Guo, *Nat Mater*, 2024, DOI: 10.1038/s41563-024-01848-6.
103. J. W. Jeong, M. K. Kim, H. Y. Cheng, W. H. Yeo, X. Huang, Y. H. Liu, Y. H. Zhang, Y. G. Huang and J. A. Rogers, *Adv Healthc Mater*, 2014, **3**, 642-648.
104. Y. Sun and X. Yu, *Ieee Sens J*, 2016, **16**, 2832-2853.
105. W. Zhou, Y. Jiang, Q. Xu, L. Chen, H. Qiao, Y.-X. Wang, J.-C. Lai, D. Zhong, Y. Zhang, W. Li, Y. Du, X. Wang, J. Lei, G. Dong, X. Guan, S. Ma, P. Kang, L. Yuan, M. Zhang, J. B. H. Tok, D. Li, Z. Bao and W. Jia, *Nature Biomedical Engineering*, 2023, **7**, 1270-1281.
106. H. Fang, K. J. Yu, C. Gloschat, Z. Yang, E. Song, C.-H. Chiang, J. Zhao, S. M. Won, S. Xu, M. Trumpis, Y. Zhong, S. W. Han, Y. Xue, D. Xu, S. W. Choi, G. Cauwenberghs, M. Kay, Y. Huang, J. Viventi, I. R. Efimov and J. A. Rogers, *Nature Biomedical Engineering*, 2017, **1**, 0038.
107. Y. S. Choi, H. Jeong, R. T. Yin, R. Avila, A. Pfenniger, J. Yoo, J. Y. Lee, A. Tzavelis, Y. J. Lee, S. W. Chen, H. S. Knight, S. Kim, H.-Y. Ahn, G. Wickerson, A. Vázquez-Guardado, E. Higbee-Dempsey, B. A. Russo, M. A. Napolitano, T. J. Holleran, L. A. Razzak, A. N. Miniovich, G. Lee, B. Geist, B. Kim, S. Han, J. A. Brennan, K. Aras, S. S. Kwak, J. Kim, E. A. Waters, X. Yang, A. Burrell, K. San Chun, C. Liu, C. Wu, A. Y. Rwei, A. N. Spann, A. Banks, D. Johnson, Z. J. Zhang, C. R. Haney, S. H. Jin, A. V. Sahakian, Y. Huang, G. D. Trachiotis, B. P. Knight, R. K. Arora, I. R. Efimov and J. A. Rogers, *Science*, 2022, **376**, 1006-1012.
108. W. Y. Jeong, M. Kwon, H. E. Choi and K. S. Kim, *Biomater Res*, 2021, **25**.
109. K. Lee, S. Park, D. H. Jo, C. S. Cho, H. Jang, J. Yi, M. Kang, J. Kim, H. Y. Jung, J. H. Kim, W. Ryu and A. Khademhosseini, *Adv Healthc Mater*, 2022, **11**.
110. K. G. Falavarjani and Q. D. Nguyen, *Eye*, 2013, **27**, 787-794.
111. M. S. Ramos, L. T. Xu, S. Singuri, J. C. C. Tafur, S. Arepalli, J. P. Ehlers, P. K. Kaiser, R. P. Singh, A. V. Rachitskaya, S. K. Srivastava, J. E. Sears, A. P. Schachat, A. S. Babiuch, S. Sharma, D. F. Martin, C. Y. Lowder, A. D. Singh, A. Yuan and A. S. Nowacki, *Ophthalmol Retina*, 2021, **5**, 625-632.
112. M. I. Van der Reis, E. C. La Heij, Y. De Jong-Hesse, P. J. Ringens, F. Hendrikse and J. S. A. G. Schouten, *Retina-J Ret Vit Dis*, 2011, **31**, 1449-1469.
113. C. Darviot, P. Hardy and M. Meunier, *J Biophotonics*, 2019, **12**.
114. G. B. Melo, N. F. S. da Cruz, G. G. Emerson, F. A. Rezende, C. H. Meyer, S. Uchiyama, J. Carpenter, H. F. Shiroma, M. E. Farah, M. Maia and E. B. Rodrigues, *Prog Retin Eye Res*, 2021, **80**.
115. R. Merani and A. P. Hunyor, *International Journal of Retina and Vitreous*, 2015, **1**, 9.
116. A. Fang, Y. F. Wang, N. Y. Guan, Y. M. Zuo, L. M. Lin, B. J. Guo, A. S. Mo, Y. L. Wu, X. R. Lin, W. X. Cai, X. F. Chen, J. J. Ye, Z. Abdelrahman, X. D. Li, H. Y. Zheng, Z. H. Wu, S. Jin, K. Xu, Y. Huang, X. S. Gu, B. Yu and X. H. Wang, *Nature Communications*, 2023, **14**.
117. H. S. Chhabra and K. Sarda, *Advanced Drug Delivery Reviews*, 2017, **120**, 41-49.
118. L. M. Li, J. F. Mu, Y. Zhang, C. Y. Zhang, T. Ma, L. Chen, T. C. Huang, J. H. Wu, J. Cao, S. Q. Feng, Y. Z. Cai, M. Han and J. Q. Gao, *Acs Nano*, 2022, **16**, 10811-10823.
119. L. M. Li, Y. Zhang, J. F. Mu, J. C. Chen, C. Y. Zhang, H. C. Cao and J. Q. Gao, *Nano Lett*, 2020, **20**, 4298-4305.
120. Z. Zhu, J. Wang, X. Pei, J. Chen, X. Wei, Y. Liu, P. Xia, Q. Wan, Z. Gu and Y. He, *Sci Adv*, 2023, **9**, eadh2213.
121. S. Baik, D. W. Kim, Y. Park, T.-J. Lee, S. Ho Bhang and C. Pang, *Nature*, 2017, **546**, 396-400.
122. R. K. Huang, X. X. Zhang, W. Z. Li, L. R. Shang, H. Wang and Y. J. Zhao, *Adv Sci*, 2021, **8**.
123. M. Parrilla, U. Detamornrat, J. Domínguez-Robles, S. Tunca, R. F. Donnelly and K. De Wael, *Acs Sensors*, 2023, **8**, 4161-4170.
124. C. Yang, T. Sheng, W. Hou, J. Zhang, L. Cheng, H. Wang, W. Liu, S. Wang, X. Yu, Y. Zhang, J. Yu and Z. Gu, *Sci Adv*, **8**, eadd3197.

View Article Online
DOI: 10.1039/D4TB00782D

125. A. Abramson, E. Caffarel-Salvador, V. Soares, D. Minahan, R. Y. Tian, X. Lu, D. Dellal, Y. Gao, S. Kim, J. Wainer, J. Collins, S. Tamang, A. Hayward, T. Yoshitake, H.-C. Lee, J. Fujimoto, J. Fels, M. R. Frederiksen, U. Rahbek, N. Roxhed, R. Langer and G. Traverso, *Nature Medicine*, 2019, **25**, 1512-1518.
126. M. Ngoepe, Y. E. Choonara, C. Tyagi, L. K. Tomar, L. C. du Toit, P. Kumar, V. M. K. Ndesendo and V. Pillay, *Sensors-Basel*, 2013, **13**, 7680-7713.
127. S. H. Sung, Y. S. Kim, D. J. Joe, B. H. Mun, B. K. You, D. H. Keum, S. K. Hahn, M. Berggren, D. Kim and K. J. Lee, *Nano Energy*, 2018, **51**, 102-112.
128. J. Koo, S. B. Kim, Y. S. Choi, Z. Xie, A. J. Bandodkar, J. Khalifeh, Y. Yan, H. Kim, M. K. Pezhouh, K. Doty, G. Lee, Y.-Y. Chen, S. M. Lee, D. D'Andrea, K. Jung, K. Lee, K. Li, S. Jo, H. Wang, J.-H. Kim, J. Kim, S.-G. Choi, W. J. Jang, Y. S. Oh, I. Park, S. S. Kwak, J.-H. Park, D. Hong, X. Feng, C.-H. Lee, A. Banks, C. Leal, H. M. Lee, Y. Huang, C. K. Franz, W. Z. Ray, M. MacEwan, S.-K. Kang and J. A. Rogers, *Sci Adv*, **6**, eabb1093.
129. Y. Zhang, F. Liu, Y. Zhang, J. Wang, D. D'Andrea, J. B. Walters, S. Li, H.-J. Yoon, M. Wu, S. Li, Z. Hu, T. Wang, J. Choi, K. Bailey, E. Dempsey, K. Zhao, A. Lantsova, Y. Bouricha, I. Huang, H. Guo, X. Ni, Y. Wu, G. Lee, F. Jiang, Y. Huang, C. K. Franz and J. A. Rogers, *Proceedings of the National Academy of Sciences*, 2023, **120**, e2217734120.
130. C. Steiger, A. Abramson, P. Nadeau, A. P. Chandrakasan, R. Langer and G. Traverso, *Nat Rev Mater*, 2019, **4**, 83-98.
131. E. Söderlind, B. Abrahamsson, F. Erlandsson, C. Wanke, V. Iordanov and C. von Corswant, *Journal of Controlled Release*, 2015, **217**, 300-307.
132. S. S. Srinivasan, A. Alshareef, A. V. Hwang, Z. Kang, J. Kuosmanen, K. Ishida, J. Jenkins, S. Liu, W. A. M. Madani, J. Lennerz, A. Hayward, J. Morimoto, N. Fitzgerald, R. Langer and G. Traverso, *Sci Robot*, **7**, eabp9066.
133. M. Vertzoni, P. Augustijns, M. Grimm, M. Koziolek, G. Lemmens, N. Parrott, C. Pentafragka, C. Reppas, J. Rubbens, J. Van Den Abeele, T. Vanuytsel, W. Weitschies and C. G. Wilson, *European Journal of Pharmaceutical Sciences*, 2019, **134**, 153-175.
134. L. Zheng, S. Guo and M. Kawanishi, *IEEE Systems Journal*, 2022, **16**, 6413-6424.
135. A. Abramson, E. Caffarel-Salvador, M. Khang, D. Dellal, D. Silverstein, Y. Gao, M. R. Frederiksen, A. Vegge, F. Hubálek, J. J. Water, A. V. Friderichsen, J. Fels, R. K. Kirk, C. Cleveland, J. Collins, S. Tamang, A. Hayward, T. Landh, S. T. Buckley, N. Roxhed, U. Rahbek, R. Langer and G. Traverso, *Science*, 2019, **363**, 611-615.
136. A. A. Al-Majed, C. M. Neumann, T. M. Brushart and T. Gordon, *The Journal of Neuroscience*, 2000, **20**, 2602.
137. Y. Jiang, Z. Zhang, Y.-X. Wang, D. Li, C.-T. Coen, E. Hwaun, G. Chen, H.-C. Wu, D. Zhong, S. Niu, W. Wang, A. Saberi, J.-C. Lai, Y. Wu, Y. Wang, A. A. Trotsyuk, K. Y. Loh, C.-C. Shih, W. Xu, K. Liang, K. Zhang, Y. Bai, G. Gurusankar, W. Hu, W. Jia, Z. Cheng, R. H. Dauskardt, G. C. Gurtner, J. B. H. Tok, K. Deisseroth, I. Soltesz and Z. Bao, *Science*, 2022, **375**, 1411-1417.
138. H. Wu, Y. Wang, H. Li, Y. Hu, Y. Liu, X. Jiang, H. Sun, F. Liu, A. Xiao, T. Chang, L. Lin, K. Yang, Z. Wang, Z. Dong, Y. Li, S. Dong, S. Wang, J. Chen, Y. Liu, D. Yin, H. Zhang, M. Liu, S. Kong, Z. Yang, X. Yu, Y. Wang, Y. Fan, L. Wang, C. Yu and L. Chang, *Nat Electron*, 2024, DOI: 10.1038/s41928-024-01138-8.
139. U. Jain, A. M. Ver Heul, S. Xiong, M. H. Gregory, E. G. Demers, J. T. Kern, C.-W. Lai, B. D. Muegge, D. A. G. Barisas, J. S. Leal-Ekman, P. Deepak, M. A. Ciorba, T.-C. Liu, D. A. Hogan, P. Debbas, J. Braun, D. P. B. McGovern, D. M. Underhill and T. S. Stappenbeck, *Science*, 2021, **371**, 1154-1159.
140. J. Schluter, J. U. Peled, B. P. Taylor, K. A. Markey, M. Smith, Y. Taur, R. Niehus, A. Staffas, A. Dai, E. Fontana, L. A. Amoretti, R. J. Wright, S. Morjaria, M. Fenelus, M. S. Pessin, N. J. Chao, M. Lew, L. Bohannon, A. Bush, A. D. Sung, T. M. Hohl, M.-A. Perales, M. R. M. van den Brink and J. B. Xavier, *Nature*, 2020, **588**, 303-307.

View Article Online
DOI: 10.1039/D4TB00782D

141. G. Lee, E. Ray, H.-J. Yoon, S. Genovese, Y. S. Choi, M.-K. Lee, S. Şahin, Y. Yan, H.-Y. Ahn, A. J. Bandodkar, J. Kim, M. Park, H. Ryu, S. S. Kwak, Y. H. Jung, A. Odabas, U. Khandpur, W. Z. Ray, M. R. MacEwan and J. A. Rogers, *Sci Adv*, **8**, eabp9169.
142. J. Koo, M. R. MacEwan, S.-K. Kang, S. M. Won, M. Stephen, P. Gamble, Z. Xie, Y. Yan, Y.-Y. Chen, J. Shin, N. Birenbaum, S. Chung, S. B. Kim, J. Khalifeh, D. V. Harburg, K. Bean, M. Paskett, J. Kim, Z. S. Zohny, S. M. Lee, R. Zhang, K. Luo, B. Ji, A. Banks, H. M. Lee, Y. Huang, W. Z. Ray and J. A. Rogers, *Nature Medicine*, 2018, **24**, 1830-1836.
143. Z. Y. Ge, W. S. Guo, Y. Tao, H. X. Sun, X. Y. Meng, L. Y. Cao, S. G. Zhang, W. Y. Liu, M. L. Akhtar, Y. Li and Y. K. Ren, *Adv Mater*, 2023, **35**.
144. Y. Jiang, A. A. Trotsyuk, S. Niu, D. Henn, K. Chen, C.-C. Shih, M. R. Larson, A. M. Mermin-Bunnell, S. Mittal, J.-C. Lai, A. Saberi, E. Beard, S. Jing, D. Zhong, S. R. Steele, K. Sun, T. Jain, E. Zhao, C. R. Neimeth, W. G. Viana, J. Tang, D. Sivaraj, J. Padmanabhan, M. Rodrigues, D. P. Perrault, A. Chattopadhyay, Z. N. Maan, M. C. Leeolou, C. A. Bonham, S. H. Kwon, H. C. Kussie, K. S. Fischer, G. Gurusankar, K. Liang, K. Zhang, R. Nag, M. P. Snyder, M. Januszyk, G. C. Gurtner and Z. Bao, *Nature Biotechnology*, 2023, **41**, 652-662.
145. P. Mostafalu, A. Tamayol, R. Rahimi, M. Ochoa, A. Khalilpour, G. Kiaee, I. K. Yazdi, S. Bagherifard, M. R. Dokmeci, B. Ziaie, S. R. Sonkusale and A. Khademhosseini, *Small*, 2018, **14**.
146. P. L. Mage, B. S. Ferguson, D. Maliniak, K. L. Ploense, T. E. Kippin and H. T. Soh, *Nature Biomedical Engineering*, 2017, **1**, 0070.
147. C. Yang, Q. Wu, J. Liu, J. Mo, X. Li, C. Yang, Z. Liu, J. Yang, L. Jiang, W. Chen, H.-j. Chen, J. Wang and X. Xie, *Nature Communications*, 2022, **13**, 2556.
148. L. E. Osborn, A. Dragomir, J. L. Betthauser, C. L. Hunt, H. H. Nguyen, R. R. Kaliki and N. V. Thakor, *Sci Robot*, 2018, **3**, eaat3818.
149. W. Wang, Y. Jiang, D. Zhong, Z. Zhang, S. Choudhury, J.-C. Lai, H. Gong, S. Niu, X. Yan, Y. Zheng, C.-C. Shih, R. Ning, Q. Lin, D. Li, Y.-H. Kim, J. Kim, Y.-X. Wang, C. Zhao, C. Xu, X. Ji, Y. Nishio, H. Lyu, J. B. H. Tok and Z. Bao, *Science*, 2023, **380**, 735-742.
150. C. M. Proctor, A. Slézia, A. Kaszas, A. Ghestem, I. del Agua, A.-M. Pappa, C. Bernard, A. Williamson and G. G. Malliaras, *Sci Adv*, **4**, eaau1291.
151. H. Joo, Y. Lee, J. Kim, J.-S. Yoo, S. Yoo, S. Kim, A. K. Arya, S. Kim, S. H. Choi, N. Lu, H. S. Lee, S. Kim, S.-T. Lee and D.-H. Kim, *Sci Adv*, **7**, eabd4639.
152. W. Ouyang, W. Lu, Y. M. Zhang, Y. M. Liu, J. U. Kim, H. X. Shen, Y. Y. Wu, H. W. Luan, K. Kilner, S. P. Lee, Y. S. Lu, Y. Y. Yang, J. Wang, Y. J. Yu, A. J. Wegener, J. A. Moreno, Z. Q. Xie, Y. X. Wu, S. M. Won, K. Kwon, C. S. Wu, W. B. Bai, H. X. Guo, T. L. Liu, H. D. Bai, G. Monti, J. Zhu, S. R. Madhvapathy, J. Trueb, M. Stanslaski, E. M. Higbee-Dempsey, I. Stepien, N. Ghoreishi-Haack, C. R. Haney, T. I. Kim, Y. G. Huang, R. Ghaffari, A. R. Banks, T. C. Jhou, C. H. Good and J. A. Rogers, *Nature Biomedical Engineering*, 2023, **7**, 1252-+.
153. J. Ausra, M. Madrid, R. T. Yin, J. Hanna, S. Arnott, J. A. Brennan, R. Peralta, D. Clausen, J. A. Bakall, I. R. Efimov and P. Gutruf, *Sci Adv*, **8**, eabq7469.
154. A. D. Mickle, S. M. Won, K. N. Noh, J. Yoon, K. W. Meacham, Y. Xue, L. A. McIlvried, B. A. Copits, V. K. Samineni, K. E. Crawford, D. H. Kim, P. Srivastava, B. H. Kim, S. Min, Y. Shiuan, Y. Yun, M. A. Payne, J. Zhang, H. Jang, Y. Li, H. H. Lai, Y. Huang, S.-I. Park, R. W. Gereau and J. A. Rogers, *Nature*, 2019, **565**, 361-365.
155. N. Noskovicova, B. Hinz and P. Pakshir, *Journal*, 2021, **10**.
156. R. J. Soto, J. R. Hall, M. D. Brown, J. B. Taylor and M. H. Schoenfisch, *Anal Chem*, 2017, **89**, 276-299.
157. E. M. Elmowafy, M. Tiboni and M. E. Soliman, *Journal of Pharmaceutical Investigation*, 2019, **49**, 347-380.
158. Y. W. Huang, L. F. Tang and Y. W. Jiang, *Ccs Chem*, 2024, DOI: 10.31635/ccschem.024.202403858.
159. D. Liu, C. Huyan, Z. B. Wang, Z. H. Guo, X. H. Zhang, H. Torun, D. Mulvihill, B. B. Xu and F. Chen, *Mater Horiz*, 2023, **10**, 2800-2823.

View Article Online
DOI: 10.1039/D4TB00782D

160. C. Bernhard, S. J. Roeters, J. Franz, T. Weidner, M. Bonn and G. Gonella, *Physical Chemistry Chemical Physics*, 2017, **19**, 28182-28188.
161. J. Peña-Bahamonde, H. N. Nguyen, S. K. Fanourakis and D. F. Rodrigues, *Journal of Nanobiotechnology*, 2018, **16**, 75.
162. S. Jadoun, *Biomedical Materials & Devices*, 2024, **2**, 225-240.
163. Y. Maeda, M. Sekine and T. Tamura, *Journal of Medical Systems*, 2011, **35**, 969-976.
164. D. Seok, S. Lee, M. Kim, J. Cho and C. Kim, *Front Electron*, 2021, **2**.
165. S. Driessen, A. Napp, K. Schmiedchen, T. Kraus and D. Stunder, *EP Europace*, 2019, **21**, 219-229.
166. T. Campi, S. Cruciani, F. Maradei and M. Feliziani, *Journal*, 2023, **16**.
167. J. Kewcharoen, K. Shah, R. Bhardwaj, T. Contractor, M. K. Turagam, R. Mandapati, D. Lakkireddy and J. Garg, *Journal of Interventional Cardiac Electrophysiology*, 2024, DOI: 10.1007/s10840-024-01777-z.
168. Z. Zhang, O. W. Savolainen and T. G. Constandinou, *J Neural Eng*, 2022, **19**.
169. M. M. Shuvo, T. Titirsha, N. Amin and S. K. Islam, *Journal*, 2022, **15**.
170. M. Hamid Elsheikh, D. A. Shnawah, M. F. M. Sabri, S. B. M. Said, M. Haji Hassan, M. B. Ali Bashir and M. Mohamad, *Renewable and Sustainable Energy Reviews*, 2014, **30**, 337-355.
171. F. Ali, W. Raza, X. Li, H. Gul and K.-H. Kim, *Nano Energy*, 2019, **57**, 879-902.
172. F.-R. Fan, Z.-Q. Tian and Z. Lin Wang, *Nano Energy*, 2012, **1**, 328-334.
173. L. R. G. Palacios and A. G. Bracamonte, *Rsc Adv*, 2022, **12**, 12806-12822.
174. D. Darvill, A. Centeno and F. Xie, *Phys Chem Chem Phys*, 2013, **15**, 15709-15726.
175. C. Salinas and A. G. Bracamonte, 2019.
176. C. Salinas and G. Bracamonte, *Front. Drug Chem. Clin. Res*, 2018, **1**, 1-8.
177. J.-L. Tambasco, G. Corrielli, R. J. Chapman, A. Crespi, O. Zilberberg, R. Osellame and A. Peruzzo, *Sci Adv*, **4**, eaat3187.
178. J. Shi, N. Zhao, D. Yan, J. Song, W. Fu and Z. Li, *Journal of Materials Chemistry A*, 2020, **8**, 5943-5951.
179. W. Yang, Y. Qin, Z. Wang, T. Yu and Z. Ge, *J Electron Mater*, 2022, **51**, 6735-6769.
180. Q. Ou and J. Tang, *Plasmonics*, 2023, DOI: 10.1007/s11468-023-02178-0.
181. M. Sasaki, W. Xu, Y. Koga, Y. Okazawa, A. Wada, I. Shimizu and T. Niidome, *Materials*, 2022, **15**, 3132.
182. F. O. Kolawole, O. S. Kolade, S. A. Bello, S. K. Kolawole, A. T. Ayeni, T. F. Elijah, S. G. Borisade and A. P. Tschiptschin, *Int J Adv Manuf Tech*, 2023, **126**, 2295-2322.
183. U. Mahajan, M. Dhonde, K. Sahu, P. Ghosh and P. M. Shirage, *Mater Adv*, 2024, **5**, 846-895.

View Article Online
DOI: 10.1039/D4TB00782D

Data Availability Statement

This review article synthesizes and discusses information from previously published studies. No primary data were generated or analyzed in the course of this review. All data supporting the findings of this study are included within the article and its references.